A STABILIZED MIXED THREE-FIELD FORMULATION FOR STRESS ACCURATE ANALYSIS INCLUDING THE INCOMPRESSIBLE LIMIT IN FINITE STRAIN SOLID DYNAMICS

INOCENCIO CASTAÑAR[§], RAMON CODINA[§,‡] AND JOAN BAIGES[§,‡]

Abstract. *In this work a new methodology for finite strain solid dynamics problems for stress accurate analysis including the incompressible limit is presented. In previous works, the authors have presented the stabilized mixed displacement/pressure formulation to deal with the incompressibility constraint in finite strain solid dynamics. To this end, the momentum equation is complemented with a constitutive law for the pressure which emerges from the deviatoric/volumetric decomposition of the strain energy function for any hyperelastic material model. The incompressible limit is attained automatically depending on the material bulk modulus. This work exploits the concept of mixed methods to formulate stable displacement/pressure/deviatoric stress finite elements. The final goal is to design a finite element technology able to tackle simultaneously problems which may involve incompressible behavior together with a high degree of accuracy of the stress field. The Variational Multi-Scale stabilization technique and, in particular, the Orthogonal Subgrid Scale method allows the use of equal-order interpolations. These stabilization procedures lead to discrete problems which are fully stable, free of volumetric locking, stress oscillations and pressure fluctuations. Numerical benchmarks show that the results obtained compare very favorably with those obtained with the corresponding stabilized mixed displacement/pressure formulation.*

Keywords: Incompressible hyperelasticity, Solid dynamics, Mixed interpolations, Stabilization methods, Orthogonal subgrid scales.

1. INTRODUCTION

Several industrial manufacturing processes such as metal forming, forging, or friction stir welding among many others require, at the same time, stress accuracy and performance in the incompressible limit [1, 2]. It becomes crucial in these cases to use a finite element (FE) technology capable of dealing with complex phenomena such as strain localization [3], the formation of shear bands, the prediction of crack propagation [4] or the isochoric behavior of the inelastic strains [5].

Incompressibility is a widely accepted assumption used in continuum and computational mechanics [6]. In biomechanics, several materials can be modeled as nearly or fully incompressible [7]. Stress accuracy enhancement becomes very useful in many fields, such as cardiac electromechanics [8, 9] in which stress tensor acts as the coupling field with the equations describing electrical propagation in stress-assisted diffusion models [10].

Displacement-based low order FE methods perform poorly in such nearly and fully incompressible scenarios [11]. Volumetric and shear locking, pressure fluctuations and poor performance in bending dominated cases are some of the effects that are often found [12]. Popular solutions to tackle the nearly incompressible limit in the solid mechanics community are reduced and selective integration techniques [13], the B-bar and the F-bar

Date: October 13, 2023.

§ Universitat Politècnica de Catalunya, Barcelona Tech, Jordi Girona 1-3, Edifici C1, 08034 Barcelona, Spain.

‡ Centre Internacional de Mètodes Numèrics en Enginyeria (CIMNE), Edifici C1, Campus Nord UPC, Gran Capitán S/N, 08034 Barcelona, Spain.

E-mails: icastanar@cimne.upc.edu (IC),ramon.codina@upc.edu (RC), joan.baiges@upc.edu (JB).

methods [14] or the well-known mean dilatation FE method, which avoid these numerical instabilities by reducing the evaluation of the incompressibility constraints at quadrature points. However, these strategies are only designed to work with structured hexahedral meshes and they are not able to tackle the fully incompressible regime.

Mixed formulations are well established and regularly used to avoid these instabilities. The use of different stabilization techniques, and particularly those based on the Variational Multi-Scale (VMS) framework [15], allows for the use of equal-order interpolations for all master fields. A particular formulation of this type, namely, the Orthogonal Subgrid Scale (OSGS) method [16], was used in [17] to design a stabilized FE formulation for the three-field linear Stokes problem, using displacements, pressure and deviatoric stresses as variables. The analysis and FE approximation of Darcy's problem presented in [18] motivated the introduction of both strains/displacements and stresses/displacements pairs as primary variables in [19] for infinitesimal strain elasticity; in this particular case, one can change the functional framework to increase the accuracy in the calculation of the stresses. To tackle the incompressible limit, the pressure needs to be introduced as a variable [20, 21, 22], although it is also possible to design a formulation using the volumetric strain as unknown [23]. Formulations including stresses as unknowns produce a considerable increase in the number of unknowns per node, but they also increase the accuracy for strains and stresses. Furthermore, in [24] the idea of using a three-field displacement/pressure/deviatoric stress formulation was tested and seen to be very effective when solving incompressible cases in which accurate results for stress and strain fields are required. These FE technologies have demonstrated enhanced stress accuracy as well as the ability to capture stress concentrations and strain localizations guaranteeing stress convergence upon mesh refinement for first order elements.

Mixed formulations are also applied under the transient finite strain assumption. In [25, 26] the velocity/pressure pair is taken as unknown of the problem and the displacement field is updated explicitly as a final step. The problem is stabilized with the VMS framework. A family of first-order form of the equations is presented in [27, 28, 29, 30, 31, 32] where the authors propose to use as primary variables the linear momentum $\boldsymbol{p}$, the deformation gradient $\mathbf{F}$, the cofactor tensor of the deformation gradient $\mathbf{H}$ and the jacobian J; the objective for this choice of variables is to ease dealing with some complex constitutive laws, and in particular with polyconvex hyperelastic potentials. In [33] the incompressibility of the material is treated with the displacement/pressure pair in an updated Lagrangian formulation framework. Another possibility is to consider Finite Volume schemes to present a conservative cell-centered Lagrangian Finite Volume scheme for solving the hyperelasticity equations on unstructured multidimensional grids [34].

In previous works, the authors have applied stabilized mixed formulations for elasticity. Lately, a stabilized mixed displacement/pressure was presented in [35] for both nearly and fully incompressible hyperelastic material models. The system was stabilized by means of the VMS framework. The present work makes a step forward introducing a mixed three-field formulation based on displacement/pressure/deviatoric stress[1] elements with equal-order interpolations for all master fields. The only requirement is the introduction of the constitutive law for deviatoric stresses in the system of equations to be solved. This technology is expected to enhance stress accuracy as well as to increase the ability to capture stress concentrations with the guarantee of stress convergence upon mesh refinement.

This work is organized as follows: In Section 2 the solid dynamics equations in finite strain theory are summarized and a novel mixed three-field formulation is developed. Furthermore, the variational form of the problem, its linearization and several employed time integrators are introduced. In Section 3 some VMS stabilization techniques are presented and the resulting stabilized forms of the three-field formulation are shown. In Section 4

[1]As it will be shown, the stress used as unknown is deviatoric in the deformed configuration only.

several benchmarks and numerical examples are tested to assess the present formulation and to validate its performance. Also a comparison with its two-field formulation counterpart are highlighted. To end up, in Section 5 some conclusions of the proposed formulation are drawn.

2. SOLID DYNAMICS PROBLEM

In this work we employ index notation to identify a vector or tensor with its Cartesian coordinates, either in the reference or the deformed configuration. As usual, repeated indexes imply summation for all space dimensions (see e.g. [6]). To denote scalar, vector and tensor quantities we use uppercase letters when they are evaluated in the reference configuration and lowercase letters if they are reckoned in the deformed one. We employ the index zero for quantities acting in the reference configuration.

2.1. **Conservation equations.** Let $\Omega_0 \coloneqq \Omega(0)$ be an open, bounded and polyhedral domain of $\mathbb{R}^d$, where $d \in \{2,3\}$ is the number of space dimensions. The initial configuration of the body is Ω_0, whereas the current configuration of the body at time t is denoted by $\Omega(t)$. The motion is described by a function $\boldsymbol{\psi}$ which links a material particle $\mathbf{X} \in \Omega_0$ to the spatial configuration $\mathbf{x} \in \Omega(t)$ according to

$$\boldsymbol{\psi} : \Omega_0 \longrightarrow \Omega(t), \quad \mathbf{x} = \boldsymbol{\psi}(\mathbf{X}, t), \quad \forall \mathbf{X} \in \Omega_0, \quad t \geq 0.$$

The boundary of the reference configuration is denoted as $\Gamma_0 \coloneqq \partial\Omega_0$ and $\Gamma(t) \coloneqq \partial\Omega(t)$ represents the boundary of the current configuration at time t. We always assume that the mapping between both boundaries is defined through the motion, i.e., $\boldsymbol{\psi}(\Gamma_0, t) = \Gamma(t)$. We denote as $]0,T[$ the time interval of analysis.

The conservation of linear momentum in finite strain theory in a total Lagrangian formulation framework reads as

$$\rho_0 \frac{\partial^2 u_a}{\partial t^2} - \frac{\partial}{\partial X_A}\{F_{aB} S_{BA}\} = \rho_0 b_a \quad \text{in } \Omega_0 \times]0,\mathrm{T}[\,, \tag{1}$$

where ρ_0 is the initial density, $\mathbf{F} = \frac{\partial \mathbf{x}}{\partial \mathbf{X}}$ is the deformation gradient, $\mathbf{S}$ is the second Piola-Kirchhoff (PK2) stress tensor and $\rho_0 \mathbf{b}$ are the body forces. Mass conservation implies that

$$\rho J = \rho_0, \tag{2}$$

where ρ is the density at time t and $J = \det \mathbf{F} > 0$ is the Jacobian of $\mathbf{F}$. With regards to the balance of angular momentum, it implies that the PK2 stress tensor must be symmetric.

The objective of this work is to obtain a mixed formulation for stress accurate analysis including the incompressible limit. The volumetric/deviatoric split *of the Cauchy stress tensor* $\boldsymbol{\sigma}$ is the starting point to develop such formulation:

$$\boldsymbol{\sigma} = \boldsymbol{\sigma}^{\mathrm{dev}} - p\mathbf{I}, \tag{3}$$

where $\boldsymbol{\sigma}^{\mathrm{dev}}$ is the deviatoric part of $\boldsymbol{\sigma}$, p is the pressure and $\mathbf{I}$ the second-order identity tensor. We can now use the relation between stresses to obtain a proper decomposition for the PK2 stress tensor [36]:

$$S_{AB} = J F^{-1}_{Aa} F^{-1}_{Bb} \sigma_{ab} \overset{(3)}{=} J F^{-1}_{Aa} F^{-1}_{Bb} \sigma^{\mathrm{dev}}_{ab} - pJC^{-1}_{AB} \coloneqq S'_{AB} - pJC^{-1}_{AB}, \tag{4}$$

where we have introduced the 'deviatoric' PK2 stresses $\mathbf{S}'$ (see Remark 2.1 below) and the right Cauchy-Green tensor $\mathbf{C} = \mathbf{F}^T\mathbf{F}$.

Thanks to the decomposition in Eq. (4), the conservation of linear momentum can be reformulated as

$$\rho_0 \frac{\partial^2 u_a}{\partial t^2} - \frac{\partial}{\partial X_A}\left\{F_{aB} S'_{BA}\right\} + \frac{\partial}{\partial X_A}\left\{pJF^{-1}_{Aa}\right\} = \rho_0 b_a \quad \text{in } \Omega_0 \times]0,\mathrm{T}[\,. \tag{5}$$

Remark 2.1. *Tensor* $\mathbf{S}'$ *is often referred to as the 'true' deviatoric component of* $\mathbf{S}$*. The trace of* $\boldsymbol{\sigma}^{\text{dev}}$ *is zero by construction. However, it does not imply that the trace of* $\mathbf{S}'$ *also vanishes, and thus* $\mathbf{S}'$ *is not deviatoric in the algebraic sense. In fact, the 'true' deviatoric component of* $\mathbf{S}$ *satisfies the following equation (see for instance* [36]*):*

$$\mathbf{S}' : \mathbf{C} = 0, \tag{6}$$

which can be interpreted as the trace with respect to the metric tensor $\mathbf{C}$*. The above equation enables the hydrostatic pressure* p *to be evaluated directly from* $\mathbf{S}$ *as*

$$p = \frac{1}{3J}\mathbf{S} : \mathbf{C}. \tag{7}$$

2.2. **Constitutive model.** Let us restrict ourselves to nonlinear isotropic hyperelastic models (see [6, 11, 36] for further details). These models postulate the existence of a Helmholtz free-energy function (or strain energy function) Ψ. The PK2 stress tensor can be derived by taking derivatives of the Helmholtz free-energy functional with respect to the right Cauchy-Green tensor, namely

$$\mathbf{S} = 2\frac{\partial \Psi\left(\mathbf{C}\right)}{\partial \mathbf{C}}. \tag{8}$$

We want to deal with compressible models that can reach the incompressible limit case. To characterize such models, it is convenient to adopt a decoupled representation of the strain energy function of the specific form

$$\Psi\left(\mathbf{C}\right) = W\left(\bar{\mathbf{C}}\right) + U\left(J\right), \tag{9}$$

where $\bar{\mathbf{C}} = J^{-2/3}\mathbf{C}$ is the volume-preserving part of $\mathbf{C}$. Let us remark that this decomposition allows one to split the elastic response of the material into the so-called deviatoric and volumetric parts, respectively, measured in the initial configuration. We can now derive the PK2 stress tensor as

$$\mathbf{S} = 2\frac{\partial \Psi}{\partial \mathbf{C}} = 2\frac{\partial W}{\partial \mathbf{C}} + 2\frac{\partial U}{\partial \mathbf{C}} = 2\frac{\partial W}{\partial \mathbf{C}} + \frac{dU}{dJ}J\mathbf{C}^{-1}. \tag{10}$$

By comparing this definition with Eq. (4) we obtain expressions for both the pressure and the deviatoric PK2 stress tensor

$$\mathbf{S}' = 2\frac{\partial W}{\partial \mathbf{C}} \quad \text{and} \quad p = -\frac{dU}{dJ}. \tag{11}$$

Several constitutive models for both deviatoric and volumetric components are shown in [35]. Let us just describe the ones which will be applied in this work. Readers are referred to [11, 25] for further details on this kind of models.

2.2.1. *Deviatoric models.* The strain energy density must be written in terms of the strain invariants, which are defined for the volume-preserving tensor $\bar{\mathbf{C}}$ by

$$\bar{I}_1 = \text{trace } \bar{\mathbf{C}}, \quad \bar{I}_2 = \frac{1}{2}\left[\left(\text{trace } \bar{\mathbf{C}}\right)^2 - \text{trace}\left(\bar{\mathbf{C}}^2\right)\right]. \tag{12}$$

Let us present two suitable functions for the deviatoric component of the strain energy function:

- Neo-Hookean model
  This model results from considering only the first principal invariant:

$$W\left(\bar{I}_1\right) = \frac{\mu}{2}\left(\bar{I}_1 - 3\right), \tag{13}$$

  where $\mu > 0$ is the shear modulus.

- Mooney-Rivlin model
  This model is derived considering the dependance on the second invariant as

$$W\left(\bar{I}_1,\bar{I}_2\right)=\alpha_1\left(\bar{I}_1-3\right)+\alpha_2\left(\bar{I}_2-3\right), \tag{14}$$

  where α_1 and α_2 are material parameters that must satisfy $\mu=2\left(\alpha_1+\alpha_2\right)>0$.

2.2.2. *Volumetric models.* Due to the decoupled form of the strain energy density, compressibility is accounted for by the volumetric strain energy function. Let us now show two models that depend upon the bulk modulus $\kappa=\frac{2\mu(1+\nu)}{3(1-2\nu)}$, where ν is the Poisson ratio.

- Quadratic model [37]:

$$U(J)=\frac{\kappa}{2}\left(J-1\right)^2;\quad \frac{dU}{dJ}=\kappa\left(J-1\right). \tag{15}$$

- Simo-Taylor model [38]:

$$U(J)=\frac{\kappa}{4}\left(J^2-1-2\log J\right);\quad \frac{dU}{dJ}=\frac{\kappa}{2}\left(J-\frac{1}{J}\right). \tag{16}$$

Remark 2.2. *The volumetric functions can be written as $U(J)=\kappa G(J)$. Therefore, Eq. (11) can be used to obtain a proper way to impose the incompressibility of an hyperelastic material*

$$p=-\frac{dU}{dJ}\quad\Leftrightarrow\quad p=-\kappa\frac{dG}{dJ}\quad\Leftrightarrow\quad \frac{p}{\kappa}+\frac{dG}{dJ}=0. \tag{17}$$

This equation can be applied regardless of the compressibility of the material under study. It is interesting to observe that in the incompressible limit, when Poisson's ratio $\nu\to 0.5$ (for isotropic materials) then $\kappa\to\infty$ and Eq. (17) reduces automatically to

$$\frac{dG}{dJ}=0. \tag{18}$$

Eq. (18) imposes directly that $J=1$, which is in fact the condition that a material must satisfy to be incompressible in finite strain theory.

Remark 2.3. *It is interesting to show how to impose incompressibility if the real deviatoric/volumetric decomposition of the PK2 stress tensor is considered. The following relation holds:*

$$\mathbf{S}=\mathbf{S}^{\mathrm{dev}}-p^*\mathbf{I}=\mathbf{S}'-pJ\mathbf{C}^{-1},$$

where $p^*=\frac{1}{3}\mathrm{trace}\mathbf{S}$. If we take the trace of the PK2 stress tensor, we can obtain an expression for the pseudo-pressure p^* as

$$p^*=-\frac{1}{3}\left(S'_{AA}+\kappa\frac{dG}{dJ}JC^{-1}_{AA}\right),$$

which allows us to write the volumetric component of the constitutive equation as

$$\frac{1}{\kappa}\frac{3p^*+S'_{AA}}{JC^{-1}_{AA}}+\frac{dG}{dJ}=0.$$

Taking into account the widely used decomposition of the strain energy function given by Eq. (9), it seems more natural and effective to consider the classical decomposition, which gives us simpler equations in nearly incompressible scenarios.

2.3. **Governing equations.** In this section, a novel three-field formulation is introduced. The objective is the definition of a general framework, which includes the mixed two-field formulation presented in [35] to be able to tackle the incompressible limit and introduces $\mathbf{S}'$ as primary unknown to obtain a higher accuracy in the computation of stresses in finite strain problems. To this end, let us introduce the three-field mixed $\mathbf{u}p\mathbf{S}'$ formulation. Let $\mathfrak{D} = \{(\mathbf{X}, t) \,|\, \mathbf{X} \in \Omega_0,\ 0 < t < T\}$ be the space-time domain where the problem is defined. The problem consists of finding a displacement field, $\mathbf{u} : \mathfrak{D} \longrightarrow \mathbb{R}^d$, together with a deviatoric component of the PK2 stress tensor, $\mathbf{S}' : \mathfrak{D} \longrightarrow \mathbb{R}^d \otimes \mathbb{R}^d$ and a pressure field, $p : \mathfrak{D} \longrightarrow \mathbb{R}$ such that

$$\rho_0 \frac{\partial^2 u_a}{\partial t^2} - \frac{\partial}{\partial X_A}\left\{F_{aB} S'_{BA}\right\} + \frac{\partial}{\partial X_A}\left\{pJF^{-1}_{Aa}\right\} = \rho_0 b_a \qquad \text{in } \Omega_0 \times]0, \mathrm{T}[\,, \tag{19}$$

$$\frac{p}{\kappa} + \frac{dG}{dJ} = 0 \qquad \text{in } \Omega_0 \times]0, \mathrm{T}[\,, \tag{20}$$

$$S'_{AB} - 2\frac{\partial W}{\partial C_{AB}} = 0 \qquad \text{in } \Omega_0 \times]0, \mathrm{T}[\,. \tag{21}$$

The governing equations must be supplied with initial conditions of the form $\mathbf{u} = \mathbf{u}^0$, $\frac{\partial \mathbf{u}}{\partial t} = \mathbf{v}^0$ in Ω_0 at $t = 0$, with $\mathbf{u}^0$ and $\mathbf{v}^0$ given, and a set of boundary conditions which can be split into Dirichlet boundary conditions (22), where the displacement is prescribed, or Neumann boundary conditions (23), where the value of tractions $\mathbf{t}_N$ are prescribed, i.e.:

$$\mathbf{u} = \mathbf{u}_D \quad \text{on } \Gamma_{0,D}, \tag{22}$$

$$\mathbf{n}_0 \cdot (\mathbf{F} \cdot \mathbf{S}) \overset{(4)}{=} \mathbf{n}_0 \cdot (\mathbf{F} \cdot \mathbf{S}') - pJ\mathbf{n}_0 \cdot \mathbf{F}^{-T} = \mathbf{t}_N \quad \text{on } \Gamma_{0,N}, \tag{23}$$

where $\mathbf{n}_0$ is the geometric unit outward normal vector on the boundary of the reference configuration Γ_0.

Remark 2.4. *Verifying that this formulation reduces to the three-field mixed formulation in linear elasticty when infinitesimal strains theory is considered is crucial. Regarding to the momentum equation (19), the following simplifications are obtained:*

$$F_{aB} S'_{BA} \overset{(4)}{\approx} J\sigma'_{ab} \approx \left(1 + \frac{\partial u_c}{\partial x_c}\right)\sigma'_{ab} = \sigma'_{ab} + \cancelto{\approx 0}{(\nabla \cdot \mathbf{u})\,\sigma'_{ab}} \approx \sigma'_{ab} \tag{24}$$

$$pJ\mathbf{F}^{-1} \approx p\,(1 + \nabla \cdot \mathbf{u})\,\mathbf{I} = p\mathbf{I} + \cancelto{\approx 0}{p\nabla \cdot \mathbf{u}\mathbf{I}} \approx p\mathbf{I} \tag{25}$$

and taking into account that both the reference and current configurations match, we obtain the simplified momentum equation for linear elasticity

$$\rho \frac{\partial^2 u_a}{\partial t^2} - \frac{\partial \sigma'_{ab}}{\partial x_a} + \frac{\partial p}{\partial x_a} = \rho b_a \quad \textit{in } \Omega_0 \times]0, T[\,. \tag{26}$$

With respect to the incompressibility equation (20), as it was previously mentioned, $\frac{dG}{dJ}$ is a function which imposes $J = 1$. Therefore,

$$\frac{p}{\kappa} + \frac{dG}{dJ} \approx \frac{p}{\kappa} + J - 1 \approx \frac{p}{\kappa} + (1 + \nabla \cdot \mathbf{u}) - 1 = \frac{p}{\kappa} + \nabla \cdot \mathbf{u} = 0 \tag{27}$$

which is exactly the constitutive law of the pressure when considering linear elasticity. Let us recall that in the incompressible limit $\kappa \to \infty$, and this equation will reduce automatically to

$$\nabla \cdot \mathbf{u} = 0 \tag{28}$$

which is the incompressibility condition for infinitesimal strain theory. Finally, with regards to the deviatoric constitutive law (21) we can observe that

$$\begin{aligned} \mathbf{S}' = J\mathbf{F}^{-1}\boldsymbol{\sigma}^{\mathrm{dev}}\mathbf{F}^{-T} &\approx (1 + \nabla \cdot \mathbf{u})\,(\mathbf{I} + \nabla \mathbf{u})^{-1}\,\boldsymbol{\sigma}^{\mathrm{dev}}\,(\mathbf{I} + \nabla \mathbf{u})^{-T} \\ &= \boldsymbol{\sigma}^{\mathrm{dev}} + \mathcal{O}\left(\|\mathbf{u}\|^2\right) \approx \boldsymbol{\sigma}^{\mathrm{dev}} \end{aligned} \tag{29}$$

and all the deviatoric models of the strain energy presented in this work must satisfy that, in the infinitesimal strain assumption, they recover the deviatoric constitutive law of linear elasticity when second order terms are neglected. Therefore

$$\boldsymbol{\sigma}^{\text{dev}} = 2\frac{\partial W}{\partial \mathbf{C}} \approx \mathbb{C}^{\text{dev}} : \boldsymbol{\varepsilon}, \tag{30}$$

where $\boldsymbol{\varepsilon}$ is the infinitesimal strain field and $\mathbb{C}^{\text{dev}}$ is the 4th order deviatoric constitutive tensor for isotropic linear elastic materials and it is defined as

$$\mathbb{C}^{\text{dev}} = 2\mu \left\{ \mathbb{I} - \frac{1}{3}\mathbf{I} \otimes \mathbf{I} \right\}, \tag{31}$$

where $\mathbb{I}$ is the 4th order identity tensor. With Eqs. (26, 27 and 30) we recover automatically the three-field formulation for linear elasticity presented in [24].

2.4. **Variational form of the problem.** Given a set $\omega \subset \Omega_0$, we shall use the symbol $\langle \cdot, \cdot \rangle_\omega$ to refer to the integral of the product of two functions, assuming it well-defined. The subscript is omitted when $\omega = \Omega_0$.

Let $\mathbb{V}$, $\mathbb{Q}$ and $\mathbb{T}$ be, respectively, the proper functional spaces where displacement, pressure and deviatoric PK2 stress solutions are well-defined for each fixed time $t \in]0, T[$. We denote by $\mathbb{V}_0$ functions in $\mathbb{V}$ which vanish in the Dirichlet boundary $\Gamma_{0,D}$. We shall be interested also in the spaces $\mathbb{W} \coloneqq \mathbb{V} \times \mathbb{Q} \times \mathbb{T}$ and $\mathbb{W}_0 \coloneqq \mathbb{V}_0 \times \mathbb{Q} \times \mathbb{T}$.

The variational statement of the problem is derived by testing system (19)-(21) against arbitrary test functions, $\mathbf{V} \coloneqq [\mathbf{v}, q, \mathbf{T}]^T$, $\mathbf{v} \in \mathbb{V}_0$, $q \in \mathbb{Q}$ and $\mathbf{T} \in \mathbb{T}$. The weak form of the problem reads: find $\mathbf{U} \coloneqq [\mathbf{u}, p, \mathbf{S}']^T :]0, T[\to \mathbb{W}$ such that initial conditions and the Dirichlet condition (22) are satisfied and

$$\left\langle v_a, \rho_0 \frac{\partial^2 u_a}{\partial t^2} \right\rangle + \mathcal{A}(\mathbf{U}, \mathbf{V}) = \mathcal{F}(\mathbf{V}) \quad \forall \mathbf{V} \in \mathbb{W}_0, \tag{32}$$

where $\mathcal{A}(\mathbf{U}, \mathbf{V})$ is a semilinear form defined on $\mathbb{W} \times \mathbb{W}_0$ as

$$\begin{aligned} \mathcal{A}(\mathbf{U}, \mathbf{V}) \coloneqq & \left\langle \frac{\partial v_a}{\partial X_A}, F_{aB} S'_{BA} \right\rangle - \left\langle \frac{\partial v_a}{\partial X_A}, pJF^{-1}_{Aa} \right\rangle + \left\langle q, \frac{dG}{dJ} \right\rangle \\ & + \left\langle q, \frac{p}{\kappa} \right\rangle + \left\langle T_{AB}, S'_{AB} \right\rangle - \left\langle T_{AB}, 2\frac{\partial W}{\partial C_{AB}} \right\rangle. \end{aligned} \tag{33}$$

In addition, $\mathcal{F}(\mathbf{V})$ is a linear form defined on $\mathbb{W}_0$ as

$$\mathcal{F}(\mathbf{V}) \coloneqq \langle v_a, \rho_0 b_a \rangle + \langle v_a, t_{N_a} \rangle_{\Gamma_{0,N}}. \tag{34}$$

Integration by parts has been used in order to decrease the continuity requirements of unknowns p and $\mathbf{S}'$.

2.5. **Time discretization.** In this work implicit time integrators are considered. When the material under study is either nearly or fully incompressible, the Courant-Friedrichs-Lewy condition, which involves the bulk modulus, becomes very restrictive. If explicit time integrators are considered, extremely small time steps are needed in order to satisfy it. Furthermore, in the fully incompressible case, as $\kappa \to \infty$, solving the problem with explicit time integration is not possible.

Although in principle any implicit time discretization method can be applied, it has to be taken into account that a hyperbolic system of equations of second order in time is being solved . It is important to control spurious high-frequency oscillations that might appear in the solution for both nearly and fully incompressible hyperelastic materials. As a consequence, numerical time integrators with high-frequency dissipation will be applied.

Let us now consider a partition of the time interval $[0, T]$ into N time steps of size δt, assumed to be constant.

2.5.1. *Backward differentiation formula (BDF).* Given a generic time dependent function at a time step $t^{n+1} = t^n + \delta t$, for $n = 0, 1, 2, ...$ the approximation of the time derivative of order $k = 1, 2, ...$ is written using information from already computed time instants. In our problem, we have to approximate the second time derivative of the displacement, $\frac{\partial^2 \mathbf{u}}{\partial t^2}^{n+1} := \mathbf{a}^{n+1}$. Depending on the accuracy of the method, we can select the specific formulae:

$$\begin{aligned}
&\text{BDF1}: \quad \mathbf{a}^{n+1} = \frac{1}{\delta t^2}[\mathbf{u}^{n+1} - 2\mathbf{u}^n + \mathbf{u}^{n-1}] + \mathcal{O}(\delta t),\\
&\text{BDF2}: \quad \mathbf{a}^{n+1} = \frac{1}{\delta t^2}[2\mathbf{u}^{n+1} - 5\mathbf{u}^n + 4\mathbf{u}^{n-1} - \mathbf{u}^{n-2}] + \mathcal{O}(\delta t^2).
\end{aligned}$$

2.5.2. *Newmark-β equations.* This is a popular class of time integrators [11]. In this time integration formula, the updated acceleration $\mathbf{a}^{n+1}$ and velocity $\mathbf{v}^{n+1}$ are given by:

$$\begin{aligned}
\mathbf{a}^{n+1} &\approx \frac{1}{\beta \delta t^2}[\mathbf{u}^{n+1} - \mathbf{u}^n - \delta t \mathbf{v}^n - \frac{\delta t^2}{2}(1 - 2\beta)\mathbf{a}^n],\\
\mathbf{v}^{n+1} &\approx \mathbf{v}^n + (1 - \gamma)\delta t \mathbf{a}^n + \gamma \delta t \mathbf{a}^{n+1}.
\end{aligned}$$

Here β and γ are parameters to be tuned. When $\beta = \frac{1}{4}$ and $\gamma = \frac{1}{2}$ the Newmark-β method is implicit, unconditionally stable and second-order accurate for linear problems.

Remark 2.5. *Newmark-β method is not unconditionally stable for nonlinear problems. The algorithmic energy conservation was recognized as the key to achieve stability in long term simulations according to the generalized theorem presented in* [39]. *The stability in time is further studied in* [40, 41]. *In* [42, 43] *several energy-momentum consistent time-stepping schemes are proposed for some mixed formulations in nonlinear problems.*

2.6. **Linearization.** In order to solve the problem, the system needs to be linearized so that a bilinear operator which allows to compute a correction $\delta\mathbf{U}$ of a given guess for the solution at time t^{n+1} is obtained, that we denote by $\mathbf{U}^{n+1}$. Iteration counters will be omitted to simplify the notation. After using a Newton-Raphson scheme, we obtain the following linearized form of the problem. Given $\mathbf{U}^{n+1}$ as the solution at time t^{n+1} and the previous iteration, find a correction $\delta\mathbf{U} := [\delta\mathbf{u}, \delta p, \delta\mathbf{S}']^T \in \mathbb{W}_0$ such that

$$\left\langle \mathbf{v}, \rho_0 \frac{C}{\delta t^2}\delta\mathbf{u} \right\rangle + \mathcal{B}(\delta\mathbf{U}, \mathbf{V}) = \mathcal{F}(\mathbf{V}) - \mathcal{A}\left(\mathbf{U}^{n+1}, \mathbf{V}\right) - \left\langle \mathbf{v}, \rho_0 \mathbf{a}^{n+1} \right\rangle \quad \forall \mathbf{V} \in \mathbb{W}_0, \tag{35}$$

where $\mathcal{B}(\delta\mathbf{U}, \mathbf{V})$ is the bilinear form obtained through the Newton-Raphson linearization and it is defined on $\mathbb{W}_0 \times \mathbb{W}_0$ as

$$\begin{aligned}
\mathcal{B}(\delta\mathbf{U}, \mathbf{V}) = &\left\langle \frac{\partial v_a}{\partial X_A}, \frac{\partial \delta u_a}{\partial X_B} S'_{BA} \right\rangle + \left\langle \frac{\partial v_a}{\partial X_A}, F_{aB}\delta S'_{BA} \right\rangle - \left\langle \frac{\partial v_a}{\partial X_A}, JpF^{-1}_{Bb}\frac{\partial \delta u_b}{\partial X_B}F^{-1}_{Aa} \right\rangle\\
&+ \left\langle \frac{\partial v_a}{\partial X_A}, JpF^{-1}_{Ab}\frac{\partial \delta u_b}{\partial X_B}F^{-1}_{Ba} \right\rangle - \left\langle \frac{\partial v_a}{\partial X_A}, J\delta pF^{-1}_{Aa} \right\rangle + \left\langle q, \mathrm{f}(J)F^{-1}_{Aa}\frac{\partial \delta u_a}{\partial X_A} \right\rangle\\
&+ \left\langle q, \frac{\delta p}{\kappa} \right\rangle - \left\langle T_{AB}, \mathbb{C}'_{ABCD}F_{aC}\frac{\partial \delta u_a}{\partial X_D} \right\rangle + \left\langle T_{AB}, \delta S'_{AB} \right\rangle,
\end{aligned} \tag{36}$$

where $\mathrm{f}(J)$ is a function coming from the linearization of $\frac{dG}{dJ}$ and depends upon the volumetric strain energy function into consideration and $\mathbb{C}'_{ABCD} = 2\frac{\partial^2 W}{\partial C_{AB}\partial C_{CD}}$ is the deviatoric constitutive tangent matrix which relates variations of the deviatoric PK2 stress tensor, $\delta\mathbf{S}'$, with variations of the Right Cauchy tensor, $\delta\mathbf{C}$.

Note that for every implicit time integrator presented here, we can write:

$$\left.\frac{\partial^2 \mathbf{u}}{\partial t^2}\right|_{t^{n+1}} \approx \frac{C}{\delta t^2}\delta\mathbf{u} + \mathbf{a}^{n+1},$$

where C is a coefficient depending on the time integration scheme and $\mathbf{a}^{n+1}$ is the acceleration computed at the previous iteration, which in the time discretized problem will be given by any of the expressions introduced above.

2.7. **Symmetrization.** In the way we have written the problem, it is not symmetric. To achieve symmetry[2], it is possible to modify Eq. (35) by

$$\left\langle \mathbf{v}, \rho_0 \frac{C}{\delta t^2} \delta \mathbf{u} \right\rangle + \mathcal{B}^{\text{mod}}(\delta \mathbf{U}, \mathbf{V}) = \mathcal{F}(\mathbf{V}) - \mathcal{A}^{\text{mod}}\left(\mathbf{U}^{n+1}, \mathbf{V}\right) - \left\langle \mathbf{v}, \rho_0 \mathbf{a}^{n+1} \right\rangle \quad \forall \mathbf{V} \in \mathbb{W}_0, \tag{37}$$

where $\mathcal{B}^{\text{mod}}(\delta \mathbf{U}, \mathbf{V})$ is the bilinear form defined on $\mathbb{W}_0 \times \mathbb{W}_0$ as

$$\begin{aligned} \mathcal{B}^{\text{mod}}(\delta \mathbf{U}, \mathbf{V}) = & \left\langle \frac{\partial v_a}{\partial X_A}, \frac{\partial \delta u_a}{\partial X_B} S'_{BA} \right\rangle + \left\langle \frac{\partial v_a}{\partial X_A}, F_{aB} \delta S'_{BA} \right\rangle - \left\langle \frac{\partial v_a}{\partial X_A}, J p F^{-1}_{Bb} \frac{\partial \delta u_b}{\partial X_B} F^{-1}_{Aa} \right\rangle \\ & + \left\langle \frac{\partial v_a}{\partial X_A}, J p F^{-1}_{Ab} \frac{\partial \delta u_b}{\partial X_B} F^{-1}_{Ba} \right\rangle - \left\langle \frac{\partial v_a}{\partial X_A}, J \delta p F^{-1}_{Aa} \right\rangle + \left\langle q, J F^{-1}_{Aa} \frac{\partial \delta u_a}{\partial X_A} \right\rangle \\ & + \left\langle q, \frac{J}{\mathrm{f}(J)} \frac{\delta p}{\kappa} \right\rangle - \left\langle T_{AB}, F_{aA} \frac{\partial \delta u_a}{\partial X_B} \right\rangle + \left\langle T_{AB}, \mathbb{C}'^{-1}_{ABCD} \delta S_{CD} \right\rangle, \end{aligned} \tag{38}$$

and $\mathcal{A}^{\text{mod}}(\mathbf{U}, \mathbf{V})$ is a semilinear form defined on $\mathbb{W} \times \mathbb{W}_0$ as

$$\begin{aligned} \mathcal{A}^{\text{mod}}(\mathbf{U}, \mathbf{V}) \coloneqq & \left\langle \frac{\partial v_a}{\partial X_A}, F_{aB} S'_{BA} \right\rangle - \left\langle \frac{\partial v_a}{\partial X_A}, p J F^{-1}_{Aa} \right\rangle + \left\langle q, \frac{J}{\mathrm{f}(J)} \frac{dG}{dJ} \right\rangle \\ & + \left\langle q, \frac{J}{\mathrm{f}(J)} \frac{p}{\kappa} \right\rangle + \left\langle T_{AB}, \mathbb{C}'^{-1}_{ABCD} S'_{CD} \right\rangle - \left\langle T_{AB}, \mathbb{C}'^{-1}_{ABCD} 2 \frac{\partial W}{\partial C_{CD}} \right\rangle, \end{aligned} \tag{39}$$

where we have multiplied the second equation by the linearized term $\frac{J}{\mathrm{f}(J)}$ and we have introduced $\mathbb{C}'^{-1}$ as the inverse deviatoric constitutive tangent matrix. To define such 4^{th} order tensor, it is necessary to obtain the inverse strain energy function, which involves a nonlinear problem.

In spite of this difficulty, the symmetric form of the problem can be interesting from both the theoretical and the practical point of views. From the theoretical point of view, the problem to be solved corresponds to the minimization of a certain mechanical energy, whereas from the practical point of view the symmetry can be exploited when solving the linear system. Also from the conceptual standpoint, the test functions for the constitutive equation in the non-symmetric case are in fact strains, whereas in the symmetric case they are stresses.

Let us also remark that, while in the infinitesimal strain theory it is equivalent to use stresses or strains as unknowns, in finite strain elasticity the symmetrization of the problem using strains (e.g. the Green-Lagrange strain $\mathbf{E}$) is much more involved than using the PK2 stress that we have presented. In any case, we will not discuss here the introduction of strains as unknowns of the problem.

For simplicity, we will employ the non-symmetric form of the problem in what follows, although the use of the symmetric version would be straightforward.

2.8. **Galerkin spatial discretization.** The standard Galerkin approximation of this abstract variational problem is now straightforward. Let $\mathcal{P}_h$ denote a FE partition of the domain Ω_0. The diameter of an element domain $K \in \mathcal{P}_h$ is denoted by h_K and the diameter on the FE partition by $h = \max\{h_K | K \in \mathcal{P}_h\}$. We can now construct conforming FE spaces $\mathbb{V}_h \subset \mathbb{V}$, $\mathbb{Q}_h \subset \mathbb{Q}$, $\mathbb{T}_h \subset \mathbb{T}$ and $\mathbb{W}_h = \mathbb{V}_h \times \mathbb{Q}_h \times \mathbb{T}_h$ in the usual manner, as well as the corresponding subspaces $\mathbb{V}_{h,0} \subset \mathbb{V}_0$ and $\mathbb{W}_{h,0} = \mathbb{V}_{h,0} \times \mathbb{Q}_h \times \mathbb{T}_h$, $\mathbb{V}_{h,0}$ being made of functions that vanish on the Dirichlet boundary. In principle, functions in $\mathbb{V}_h$ are continuous, whereas functions in both $\mathbb{Q}_h$ and $\mathbb{T}_h$ not necessarily.

[2]In the case of homogeneous boundary conditions, obviously.

The Galerkin discrete version of problem (35) is: for a given time t^{n+1} and a fixed iteration, find $\delta\mathbf{U}_h \coloneqq [\delta\mathbf{u}_h, \delta p_h, \delta\mathbf{S}'_h]^T \in \mathbb{W}_{h,0}$ such that

(40)
$$\left\langle \mathbf{v}_h, \rho_0 \frac{C}{\delta t^2}\delta\mathbf{u}_h \right\rangle + \mathcal{B}\left(\delta\mathbf{U}_h, \mathbf{V}_h\right) = \mathcal{F}\left(\mathbf{V}_h\right) - \mathcal{A}\left(\mathbf{U}_h^{n+1}, \mathbf{V}_h\right) - \left\langle \mathbf{v}_h, \rho_0 \mathbf{a}_h^{n+1} \right\rangle \quad \forall \mathbf{V}_h \in \mathbb{W}_{h,0}.$$

The stability of the discrete formulation depends on compatibility restrictions on the interpolation functions chosen for the displacement, deviatoric PK2 stress and pressure fields, as stated by the appropriate inf–sup condition [44]. According to these restrictions, mixed elements with continuous equal order linear interpolation for all fields are not stable. However, the inf–sup condition can be circumvented by using a stabilization technique. This is why the so-called stabilized formulations have been proposed to approximate this kind of problems. The main idea is to replace Eq. (35) by another discrete variational problem in which the bilinear form $\mathcal{B}$ is enhanced so that it has improved stability properties. In order to overcome the instabilities previously discussed, we propose the stabilization technique described in next section.

Remark 2.6. *In principle, we have posed no restrictions on the choice of the FE spaces. However, the Galerkin formulation is only stable if two inf-sup conditions are satisfied, one between the displacements and the stresses and another one between the displacements and the pressure. This conditions are explained in* [17] *for the linear Stokes problem, and are obviously inherited in the nonlinear problem considered now. Only stresses can be controlled with the Gakerkin formulation, and in the case of compressible materials also the pressure, but this control disappears as* $\kappa \to \infty$*. Displacement gradients need to be controlled using an inf-sup condition and pressures (regardless of the compressibility) using another one. The alternative to using the Galerkin method with FE spaces satisfying the inf-sup conditions is to use a stabilized FE method, as the one we describe next.*

3. SOLID DYNAMICS STABILIZED FINITE ELEMENT FORMULATION

In this work, the VMS method [15, 45] is introduced to stabilize the discrete formulation of the mixed problem allowing for the use of linear interpolations for all master fields. The basic idea of the VMS approach is to enlarge Galerkin's space of approximation, $\mathbb{W}_h$, adding a finer resolution space, $\tilde{\mathbb{W}}$, referred to as the subgrid scale (SGS) space. Let $\mathbb{W} = \mathbb{W}_h \oplus \tilde{\mathbb{W}}$. The elements of this space are denoted by $\tilde{\mathbf{U}} \coloneqq [\tilde{\mathbf{u}}, \tilde{p}, \tilde{\mathbf{S}}']^T$ and they are called SGSs. Likewise, let $\mathbb{W}_0 = \mathbb{W}_{h,0} \oplus \tilde{\mathbb{W}}_0$, where $\tilde{\mathbb{W}}_0$ is being made of displacement SGSs (defined at element level) that vanish at all the element boundaries.

Taking into account that $\mathcal{B}$ is a bilinear form, the continuous problem (40) is equivalent to find $\delta\mathbf{U}_h \in \mathbb{W}_{h,0}$ and $\tilde{\mathbf{U}} \in \tilde{\mathbb{W}}$ such that

$$\begin{aligned} &\left\langle \mathbf{v}_h, \rho_0 \frac{C}{\delta t^2}\delta\mathbf{u}_h \right\rangle + \left\langle \mathbf{v}_h, \rho_0 \tilde{\mathbf{a}}^{n+1} \right\rangle + \mathcal{B}\left(\delta\mathbf{U}_h, \mathbf{V}_h\right) + \mathcal{B}\left(\tilde{\mathbf{U}}, \mathbf{V}_h\right) \\ &\qquad = \mathcal{F}\left(\mathbf{V}_h\right) - \mathcal{A}\left(\mathbf{U}_h^{n+1}, \mathbf{V}_h\right) - \left\langle \mathbf{v}_h, \rho_0 \mathbf{a}_h^{n+1} \right\rangle \quad \forall \mathbf{V}_h \in \mathbb{W}_{h,0}, \end{aligned} \tag{41}$$

$$\begin{aligned} &\left\langle \tilde{\mathbf{v}}, \rho_0 \frac{C}{\delta t^2}\delta\mathbf{u}_h \right\rangle + \left\langle \tilde{\mathbf{v}}, \rho_0 \tilde{\mathbf{a}}^{n+1} \right\rangle + \mathcal{B}\left(\delta\mathbf{U}_h, \tilde{\mathbf{V}}\right) + \mathcal{B}\left(\tilde{\mathbf{U}}, \tilde{\mathbf{V}}\right) \\ &\qquad = \mathcal{F}\left(\tilde{\mathbf{V}}\right) - \mathcal{A}\left(\mathbf{U}_h^{n+1}, \tilde{\mathbf{V}}\right) - \left\langle \tilde{\mathbf{v}}, \rho_0 \mathbf{a}_h^{n+1} \right\rangle \quad \forall \tilde{\mathbf{V}} \in \tilde{\mathbb{W}}, \end{aligned} \tag{42}$$

where Eq. (41) is called the FE scale equation and Eq. (42) is called the SGS equation. The approximation to the acceleration obtained from the displacement SGS at time t^{n+1} has been denoted by $\tilde{\mathbf{a}}^{n+1}$.

The main idea behind any stabilized FE method derived from the VMS framework is to obtain an expression for the SGSs from the SGS equation in order to complement our FE scale equation. First of all let us make some assumptions about the SGS functions.

In this work we consider the SGSs to be quasi-static, which means that we neglect their time derivative. We also assume the SGSs to behave as bubble functions, which means that their velocity component vanishes across inter-element boundaries. Taking this into account, we can integrate by parts within each element in Eq. (42) to obtain:

$$\begin{aligned}&\sum_K \left\langle \tilde{\mathbf{v}}, \rho_0 \frac{C}{\delta t^2}\delta \mathbf{u}_h \right\rangle_K + \sum_K \left\langle \tilde{\mathbf{V}}, \mathrm{B}\left(\delta \mathbf{U}_h\right)\right\rangle_K + \sum_K \left\langle \tilde{\mathbf{V}}, \mathrm{B}\left(\tilde{\mathbf{U}}\right)\right\rangle_K \\ &\qquad = \sum_K \left\langle \tilde{\mathbf{V}}, \mathrm{F}\right\rangle_K - \sum_K \left\langle \tilde{\mathbf{V}}, \mathrm{A}\left(\mathbf{U}_h^{n+1}\right)\right\rangle_K - \sum_K \left\langle \tilde{\mathbf{v}}, \rho_0 \mathbf{a}_h^{n+1}\right\rangle_K \quad \forall \tilde{\mathbf{V}} \in \tilde{\mathbb{W}},\end{aligned} \tag{43}$$

where $\sum_K$ stands for the summation over all $K \in \mathcal{P}_h$ and $\mathrm{B} = [\mathrm{B}_u, \mathrm{B}_p, \mathrm{B}_S]^T$ is a linear operator coming from the integration by parts of $\mathcal{B}$ such that $\mathcal{B}\left(\delta \mathbf{U}_h, \tilde{\mathbf{V}}\right) = \sum_K \left\langle \tilde{\mathbf{V}}, \mathrm{B}\left(\delta \mathbf{U}_h\right)\right\rangle_K$ and it is defined as

$$\begin{aligned}\mathrm{B}_u\left(\delta \mathbf{U}_h\right)_a = &-\frac{\partial}{\partial X_A}\left\{\frac{\partial \delta u_{h_a}}{\partial X_B} S'_{AB}\right\} - \frac{\partial}{\partial X_A}\left\{F_{aB}\delta S'_{h_{AB}}\right\} \\ &+ \frac{\partial}{\partial X_A}\left\{Jp F^{-1}_{Bb}\frac{\partial \delta u_{h_b}}{\partial X_B}F^{-1}_{Aa}\right\} - \frac{\partial}{\partial X_A}\left\{Jp F^{-1}_{Ab}\frac{\partial \delta u_{h_b}}{\partial X_B}F^{-1}_{Ba}\right\} \\ &+ \frac{\partial}{\partial X_A}\left\{J\delta p_h F^{-1}_{Aa}\right\},\end{aligned} \tag{44}$$

$$\mathrm{B}_p\left(\delta \mathbf{U}_h\right) = \mathrm{f}\left(J\right) F^{-1}_{Aa}\frac{\partial \delta u_{h_a}}{\partial X_A} + \frac{\delta p_h}{\kappa}, \tag{45}$$

$$\mathrm{B}_S\left(\delta \mathbf{U}_h\right)_{AB} = -\mathbb{C}'_{ABCD}F_{aC}\frac{\partial \delta u_{h_a}}{\partial X_D} + \delta S'_{h_{AB}}. \tag{46}$$

Regarding the right-hand side, $\mathrm{F} = [\mathrm{F}_u, \mathrm{F}_p, \mathrm{F}_S]^T$ appears from the external forces form $\mathcal{F}$ and it is given by

$$\mathrm{F}_{u_a} = \rho_0 b_a \quad ; \quad \mathrm{F}_p = 0 \quad ; \quad \mathrm{F}_{S_{AB}} = 0, \tag{47}$$

and finally $\mathrm{A}\left(\mathbf{U}_h^{n+1}\right) = \left[\mathrm{A}_u\left(\mathbf{U}_h^{n+1}\right), \mathrm{A}_p\left(\mathbf{U}_h^{n+1}\right), \mathrm{A}_S\left(\mathbf{U}_h^{n+1}\right)\right]^T$ comes from the integration by parts of $\mathcal{A}$ and it is defined as

$$\mathrm{A}_u\left(\mathbf{U}_h^{n+1}\right)_a = -\frac{\partial}{\partial X_A}\{F_{aB}S'_{BA}\} + \frac{\partial}{\partial X_A}\{Jp F^{-1}_{Aa}\}, \tag{48}$$

$$\mathrm{A}_p\left(\mathbf{U}_h^{n+1}\right) = \frac{dG}{dJ} + \frac{p}{\kappa}, \tag{49}$$

$$\mathrm{A}_S\left(\mathbf{U}_h^{n+1}\right)_{AB} = S'_{AB} - 2\frac{\partial W}{\partial C_{AB}}. \tag{50}$$

Eq. (43) must be satisfied for all elements $K \in \mathcal{P}_h$ and for any $\tilde{\mathbf{V}} \in \tilde{\mathbb{W}}$, which strictly enforces that

$$\tilde{\Pi}\left(\mathrm{B}\left(\delta \mathbf{U}_h\right) + \mathrm{B}\left(\tilde{\mathbf{U}}\right)\right) = \tilde{\Pi}\left(\mathrm{F} - \mathrm{A}\left(\mathbf{U}_h^{n+1}\right)\right), \tag{51}$$

where $\tilde{\Pi}$ is the $L^2(\Omega_0)$ projection onto the SGS space. This equation allows us to obtain an expression for the SGSs:

$$\tilde{\Pi}\left(\mathrm{B}\left(\tilde{\mathbf{U}}\right)\right) = \tilde{\Pi}\left(\mathrm{F} - \mathrm{A}\left(\mathbf{U}_h^{n+1}\right) - \mathrm{B}\left(\delta \mathbf{U}_h\right)\right) \coloneqq \tilde{\Pi}\left(\mathrm{R}\left(\mathbf{U}_h^{n+1}\right) + \mathrm{R}_{\delta \mathbf{U}}\left(\delta \mathbf{U}_h\right)\right), \tag{52}$$

where the residuals are defined as $\mathrm{R}_{\delta \mathbf{U}}\left(\delta \mathbf{U}_h\right) \coloneqq -\mathrm{B}\left(\delta \mathbf{U}_h\right)$ and $\mathrm{R}\left(\mathbf{U}_h^{n+1}\right) \coloneqq \mathrm{F} - \mathrm{A}\left(\mathbf{U}_h^{n+1}\right)$.

The idea now is to approximate operator B by a matrix $\boldsymbol{\tau}_K^{-1}$ within each element K. Since we may consider that $\boldsymbol{\tau}_K^{-1}\tilde{\mathbf{U}}$ already belongs to the SGS space, $\tilde{\Pi}\left(\boldsymbol{\tau}_K^{-1}\tilde{\mathbf{U}}\right) = \boldsymbol{\tau}_K^{-1}\tilde{\mathbf{U}}$,

and from Eq. (52) we obtain

$$\tilde{\mathbf{U}} \approx \boldsymbol{\tau}_K \tilde{\Pi} \left(\mathrm{R} \left(\mathbf{U}_h^{n+1} \right) + \mathrm{R}_{\delta \mathbf{U}} \left(\delta \mathbf{U}_h \right) \right) \quad \text{in } K \in \mathcal{P}_h, \tag{53}$$

where $\boldsymbol{\tau}_K$ is a matrix of algorithmic parameters depending on K and the operator B. This approximation for $\tilde{\mathbf{U}}$ is intended to mimic the effect of $\mathrm{B}\left(\tilde{\mathbf{U}}\right)$ in the volume integral (41). Let us remark that $\boldsymbol{\tau}_K$ is taken as a diagonal matrix of stabilization parameters, $\boldsymbol{\tau}_K = \mathrm{diag}\left(\tau_u \boldsymbol{I}_d, \tau_p, \tau_S \boldsymbol{I}\right)$, with $\boldsymbol{I}_d$ the identity on vectors of $\mathbb{R}^d$ and parameters τ_u, τ_p and τ_S are coefficients coming from the study of the behavior of the stabilization parameters based on a Fourier analysis of the problem for the SGSs. In this work, we propose to use the stabilization parameters presented in [24] for linear elastic cases:

$$\tau_u = c_1 \frac{h_K^2}{2\mu} \quad \text{and} \quad \tau_p = 2 c_2 \mu \quad \text{and} \quad \tau_S = c_3, \tag{54}$$

where c_1, c_2 and c_3 are algorithmic parameters which must be determined.

Finally, Eq. (53) can be introduced into the FE scale equation to obtain the following stabilized weak form

$$\begin{aligned} &\left\langle \mathbf{v}_h, \rho_0 \frac{C}{\delta t^2} \delta \mathbf{u}_h \right\rangle + \mathcal{B}\left(\delta \mathbf{U}_h, \mathbf{V}_h\right) + \sum_K \boldsymbol{\tau}_K \left\langle \mathrm{L}\left(\mathbf{V}_h\right), \tilde{\Pi}\left(\mathrm{R}\left(\mathbf{U}_h^{n+1}\right) + \mathrm{R}_{\delta \mathbf{U}}\left(\delta \mathbf{U}_h\right)\right)\right\rangle \\ &\qquad = \mathcal{F}\left(\mathbf{V}_h\right) - \mathcal{A}\left(\mathbf{U}_h^{n+1}, \mathbf{V}_h\right) - \left\langle \mathbf{v}_h, \rho_0 \mathbf{a}_h^{n+1} \right\rangle \quad \forall \mathbf{V}_h \in \mathbb{W}_{h,0}, \end{aligned} \tag{55}$$

where $\mathrm{L}\left(\mathbf{V}_h\right) = \left[\mathrm{L}_u\left(\mathbf{V}_h\right), \mathrm{L}_p\left(\mathbf{V}_h\right), \mathrm{L}_S\left(\mathbf{V}_h\right)\right]^T$ is a linear operator coming from the integration by parts of $\mathcal{B}$ such that $\mathcal{B}\left(\tilde{\mathbf{U}}, \mathbf{V}_h\right) = \sum_K \left\langle \mathrm{L}\left(\mathbf{V}_h\right), \tilde{\mathbf{U}} \right\rangle_K$ and it is defined as

$$\begin{aligned} \mathrm{L}_u\left(\mathbf{V}_h\right)_a = &- \frac{\partial}{\partial X_A}\left\{ \frac{\partial v_{h_a}}{\partial X_B} S'_{AB} \right\} + \frac{\partial}{\partial X_A}\left\{ J p F^{-1}_{Aa} \frac{\partial v_{h_b}}{\partial X_B} F^{-1}_{Bb} \right\} \\ &- \frac{\partial}{\partial X_A}\left\{ J p F^{-1}_{Ba} \frac{\partial v_{h_b}}{\partial X_B} F^{-1}_{Ab} \right\} - \frac{\partial}{\partial X_A}\left\{ q f(J) F^{-1}_{Aa} \right\} \\ &+ \frac{\partial}{\partial X_D}\left\{ T_{AB} \mathbb{C}'_{ABCD} F_{aC} \right\}, \end{aligned} \tag{56}$$

$$\mathrm{L}_p\left(\mathbf{V}_h\right) = \frac{\partial v_{h_a}}{\partial X_A} J F^{-1}_{Aa} + \frac{q}{\kappa}, \tag{57}$$

$$\mathrm{L}_S\left(\mathbf{V}_h\right)_{AB} = \frac{\partial v_{h_a}}{\partial X_A} F_{aB} + T_{AB}. \tag{58}$$

There exist several stabilization methods coming from the VMS technique depending on the selection of the projection onto the SGS space. In this work, three different options are considered.

Remark 3.1. *Matrix $\boldsymbol{\tau}_K$ can be understood as an algebraic approximation to the inverse of the tangent operator introduced in the linearization of the originally nonlinear problem. Therefore, different linearization strategies could lead to different stabilized FE formulations. This idea is further elaborated in* [46].

3.1. **Algebraic SubGrid Scales (ASGS).** This is the simplest choice. We take the projection onto the SGS space as the identity when applied to the residual (see [18] for further details), so that

$$\tilde{\Pi}\left(\mathrm{R}\left(\mathbf{U}_h^{n+1}\right) + \mathrm{R}_{\delta \mathbf{U}}\left(\delta \mathbf{U}_h\right)\right) = \mathrm{R}\left(\mathbf{U}_h^{n+1}\right) + \mathrm{R}_{\delta \mathbf{U}}\left(\delta \mathbf{U}_h\right), \tag{59}$$

and we obtain as a final stabilized formulation

$$\left\langle \mathbf{v}_h, \rho_0 \frac{C}{\delta t^2} \delta \mathbf{u}_h \right\rangle + \mathcal{B}\left(\delta \mathbf{U}_h, \mathbf{V}_h\right) + \sum_K \boldsymbol{\tau}_K \left\langle \mathrm{L}\left(\mathbf{V}_h\right), \mathrm{R}_{\delta \mathbf{U}}\left(\delta \mathbf{U}_h\right)\right\rangle = \mathcal{F}\left(\mathbf{V}_h\right)$$

$$-\mathcal{A}\left(\mathbf{U}_h^{n+1},\mathbf{V}_h\right)-\left\langle \mathbf{v}_h,\rho_0\mathbf{a}_h^{n+1}\right\rangle-\sum_K\boldsymbol{\tau}_K\left\langle \mathrm{L}\left(\mathbf{V}_h\right),\mathrm{R}\left(\mathbf{U}_h^{n+1}\right)\right\rangle\quad\forall\mathbf{V}_h\in\mathbb{W}_{h,0}. \tag{60}$$

3.2. **Orthogonal Subgrid Scales (OSGS).** In [47] it is argued that a natural approximation for the unknown SGS space it to take it orthogonal to the FE space:

$$\tilde{\Pi}\left(\mathrm{R}\left(\mathbf{U}_h^{n+1}\right)+\mathrm{R}_{\delta\mathbf{U}}\left(\delta\mathbf{U}_h\right)\right)=\mathrm{R}\left(\mathbf{U}_h^{n+1}\right)+\mathrm{R}_{\delta\mathbf{U}}\left(\delta\mathbf{U}_h\right)-\Pi^h\left(\mathrm{R}\left(\mathbf{U}_h^{n+1}\right)\right),$$

where Π^h is the $L^2\left(\Omega_0\right)$ projection onto the FE space. Due to the fact that this projection would increase the size of our system if we compute it in an implicit way, we have decided to approximate it with the residual of the previous iteration by neglecting the projection of the operator $\mathrm{R}_{\delta\mathbf{U}}\left(\delta\mathbf{U}_h\right)$. The final form of the stabilized problem with OSGS method emerges as

$$\begin{aligned}&\left\langle \mathbf{v}_h,\rho_0\frac{C}{\delta t^2}\delta\mathbf{u}_h\right\rangle+\mathcal{B}\left(\delta\mathbf{U}_h,\mathbf{V}_h\right)+\sum_K\boldsymbol{\tau}_K\left\langle \mathrm{L}\left(\mathbf{V}_h\right),\mathrm{R}_{\delta\mathbf{U}}\left(\delta\mathbf{U}_h\right)\right\rangle=\mathcal{F}\left(\mathbf{V}_h\right)-\mathcal{A}\left(\mathbf{U}_h^{n+1},\mathbf{V}_h\right)\\&-\left\langle \mathbf{v}_h,\rho_0\mathbf{a}_h^{n+1}\right\rangle-\sum_K\boldsymbol{\tau}_K\left\langle \mathrm{L}\left(\mathbf{V}_h\right),\mathrm{R}\left(\mathbf{U}_h^{n+1}\right)-\Pi^h\left(\mathrm{R}\left(\mathbf{U}_h^{n}\right)\right)\right\rangle\quad\forall\mathbf{V}_h\in\mathbb{W}_{h,0}.\end{aligned} \tag{61}$$

3.3. **Split Orthogonal Subgrid Scales (S-OSGS).** A key property of the OSGS stabilization is that, thanks to the projection onto the FE space, we keep the consistency of the formulation in a weak sense in spite of including just the minimum number of terms to stabilize the solution. This property allows us to propose the following split version of the OSGS method:

$$\begin{aligned}&\left\langle \mathbf{v}_h,\rho_0\frac{C}{\delta t^2}\delta\mathbf{u}_h\right\rangle+\mathcal{B}\left(\delta\mathbf{U}_h,\mathbf{V}_h\right)+\sum_K\boldsymbol{\tau}_K\left\langle \mathrm{L}^*\left(\mathbf{V}_h\right),\mathrm{R}^*_{\delta\mathbf{U}}\left(\delta\mathbf{U}_h\right)\right\rangle=\mathcal{F}\left(\mathbf{V}_h\right)-\mathcal{A}\left(\mathbf{U}_h^{n+1},\mathbf{V}_h\right)\\&-\left\langle \mathbf{v}_h,\rho_0\mathbf{a}_h^{n+1}\right\rangle-\sum_K\boldsymbol{\tau}_K\left\langle \mathrm{L}^*\left(\mathbf{V}_h\right),\mathrm{R}^*\left(\mathbf{U}_h^{n+1}\right)-\Pi^h\left(\mathrm{R}^*\left(\mathbf{U}_h^{n}\right)\right)\right\rangle\quad\forall\mathbf{V}_h\in\mathbb{W}_{h,0},\end{aligned} \tag{62}$$

where the split operators are defined as

$$\begin{aligned}&\mathrm{B}^*_u\left(\delta\mathbf{U}_h\right)_a=\frac{\partial}{\partial X_A}\left\{J\delta p_h F^{-1}_{Aa}\right\},\ \mathrm{B}^*_p\left(\delta\mathbf{U}_h\right)=0,\ \mathrm{B}^*_S\left(\delta\mathbf{U}_h\right)_{AB}=-\mathbb{C}'_{ABCD}F_{aC}\frac{\partial\delta u_{h_a}}{\partial X_D},\\&\mathrm{A}^*_u\left(\mathbf{U}_h^{n+1}\right)_a=\frac{\partial}{\partial X_A}\{JpF^{-1}_{Aa}\},\ \mathrm{A}^*_p\left(\mathbf{U}_h^{n+1}\right)=0,\ \mathrm{A}^*_S\left(\mathbf{U}_h^{n+1}\right)_{AB}=-2\frac{\partial W}{\partial C_{AB}},\\&\mathrm{L}^*_u\left(\mathbf{V}_h\right)_a=-\frac{\partial}{\partial X_A}\left\{qf(J)F^{-1}_{Aa}\right\},\ \mathrm{L}^*_p\left(\mathbf{V}_h\right)=0,\ \mathrm{L}^*_S\left(\mathbf{V}_h\right)_{AB}=\frac{\partial v_{h_a}}{\partial X_A}F_{aB}.\end{aligned}$$

The S-OSGS method is not just a simplification of the OSGS one. For smooth solutions, both have an optimal convergence rate in mesh size. However, in problems where the solution has strong gradients, we have found the S-OSGS more robust, similarly to what it is explained in [48].

4. NUMERICAL EXAMPLES

In this section, several numerical examples are presented to assess the performance of the proposed three-field formulation. As a first case, a test with a manufactured solution is considered to analyze the spatial discretization errors upon mesh refinement and the nonlinear iteration convergence error with a Newton-Raphson scheme for each unknown of the problem. Later, we consider a bending problem for a beam-like structure in order to show the behavior of the method in bending dominated scenarios. Finally, a twisting column is set which presents extreme nonlinear deformations. All these examples are widely used in incompressible hyperelastic cases [25, 26, 49, 50]. To highlight the main advantages of the presented three field mixed $\mathbf{u}p\mathbf{S}'$ formulation with respect to the two-field one presented in [35], some comparisons will be done against the stabilized mixed $\mathbf{u}p$ formulation proposed in this last reference.

For all the numerical examples included next, hyperelastic models are considered fully incompressible, and so the bulk modulus is $\kappa = \infty$, unless otherwise specified. With regards to the stabilization technique, we select the S-OSGS method except where otherwise stated. The algorithmic parameters are set to $c_1 = 1$, $c_2 = 1$ and $c_3 = 0.5$. As previously discussed, the nonlinearities in the problem are solved via a Newton-Raphson scheme. Depending on these nonlinearities, the initial guess of the iterative procedure needs to be close enough to the solution to guarantee convergence of the nonlinear iterations. In time-depending schemes, the time step is the parameter which controls the evolution of the nonlinear iterations, so we will have to tune it depending on the nonlinearities of each numerical example. A maximum of 10 iterations is set, and the numerical tolerance for the $L^2(\Omega_0)$ norm is 10^{-7}. In order to solve the monolithic system of linear equations, we use the Biconjugate Gradients solver, `BiCGstab` [51], which is already implemented in the `PETSc` parallel solver library [52].

4.1. **A test with analytical solution.** Let us first perform a simple test whose main objective is to numerically check the order of convergence of the proposed scheme with respect to the mesh size. For this purpose we use the so-called method of manufactured solutions.

In this procedure, an exact analytical solution is defined a priori and later substituted into the continuum equations in order to obtain the associated forcing terms. These forcing terms are then introduced in the FE computation. The manufactured solutions are composed of smooth functions. Dirichlet boundary conditions are prescribed over the boundaries upon evaluation of the displacement analytical solution. So as to avoid mixing both spatial and time errors, we consider static solutions.

The region we consider is the unit square plate $\Omega_0 = [0,1] \times [0,1]$ under plain strain assumption and we impose the following manufactured displacement and pressure fields:

$$\mathbf{u}(X,Y) = k\left[\exp(X+Y), -\exp(X+Y)\right], \tag{63}$$

$$p(X,Y) = \mu \sin(2\pi X)\sin(2\pi Y), \tag{64}$$

where $k = 0.01$ and X and Y referring to the Cartesian axes in the reference configuration. All quantities are assumed dimensionless in this example. It is important to note that this displacement field gives an incompressible motion due to the fact that the Jacobian is $J(\mathbf{u}(X,Y)) = 1$ for all X, Y. We set a Neo-Hookean material for the deviatoric part of the stresses, with shear modulus $\mu = 3.3 \times 10^6$ and Poisson ratio $\nu = 0.5$ and a quadratic law for the volumetric response. Therefore, the manufactured deviatoric PK2 stress field is computed with respect to the manufactured displacement field as

$$\mathbf{S}(X,Y) = \mu \left\{ \mathbf{I} - \frac{1}{3}\mathrm{trace}\left[\mathbf{C}\left(\mathbf{u}(X,Y)\right)\right]\mathbf{C}^{-1}\left(\mathbf{u}(X,Y)\right) \right\}. \tag{65}$$

We study the convergence behavior of the proposed method by running the case on seven meshes obtained by refinement. The sequence is of structured grids of n^2 linear quadrilateral elements, being n the number of FEs along each side of the domain.

The normalized error has been computed in the $L^2(\Omega_0)$ norm for displacement, pressure and deviatoric PK2 stress fields with ASGS, OSGS and S-OSGS stabilization techniques. Fig. 1a shows the displacement convergence rate upon mesh size. As expected, all stabilization methods present the same slope of 2.0. With respect to both pressure and deviatoric PK2 stress fields, all methods converge with a slope of 1.5 upon mesh refinement, as it can be observed in Figs. 1c-1e. This, in fact, corresponds to a superconvergent behavior, as the theoretical order of convergence should be 1 using linear elements. In [17] it is shown for the linear problem that the convergence order for displacements is $k+1$ and for stresses and pressures it is k in the $L^2(\Omega_0)$ norm, k being the polynomial order of the FE interpolation. For the stress-displacement formulation presented in [19] one can consider

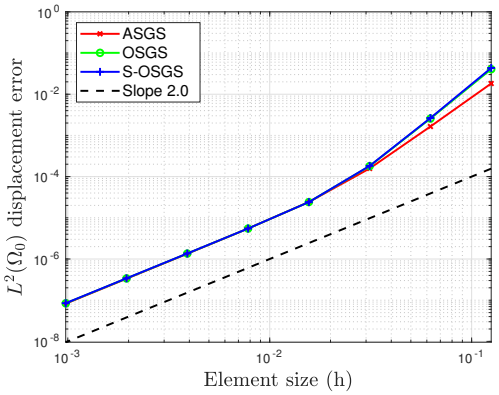

(A) Displacement error upon mesh refinement

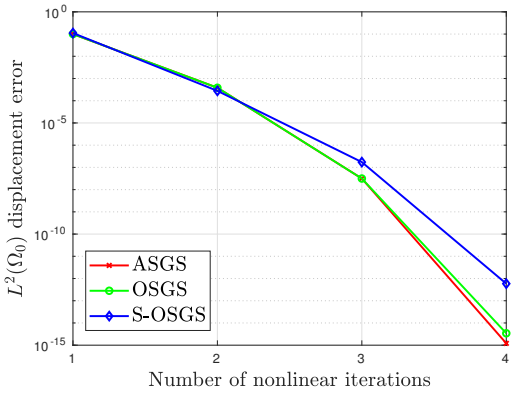

(B) Displacement nonlinear convergence error

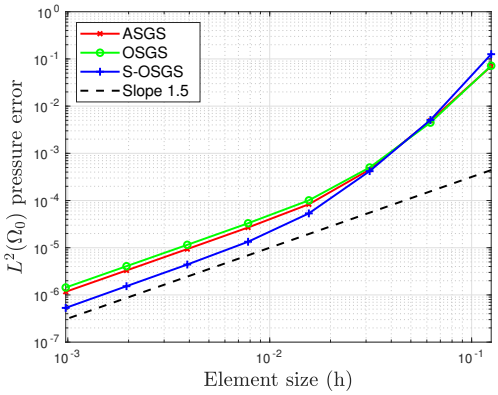

(C) Pressure error upon mesh refinement

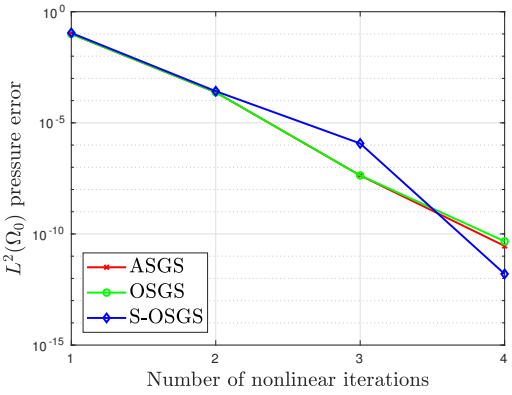

(D) Pressure nonlinear convergence error

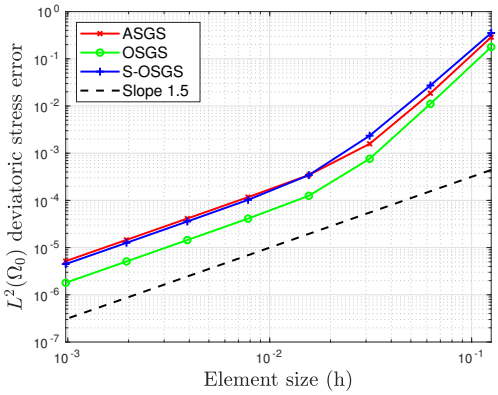

(E) Deviatoric stress error upon mesh refinement

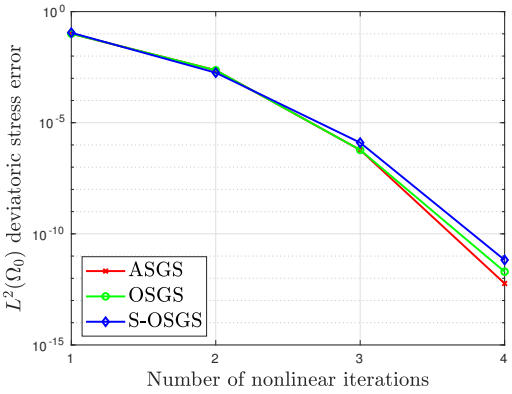

(F) Deviatoric stress nonlinear convergence error

FIGURE 1. Manufactured convergence test. Convergence rate of the $\mathbf{u}p\mathbf{S}'$ formulation upon mesh refinement and nonlinear iteration convergence error.

dual formulations and increase the order of convergence for the stresses and the expense of decreasing it for the displacements, but this is not possible when pressures are introduced as unknowns.

For the sake of completeness, Figs. 1b-1d-1f show the nonlinear iteration convergence error for each unknown of the formulation. As it can be seen, a quadratic convergence is attained thanks to the Newton-Raphson linearization of the problem.

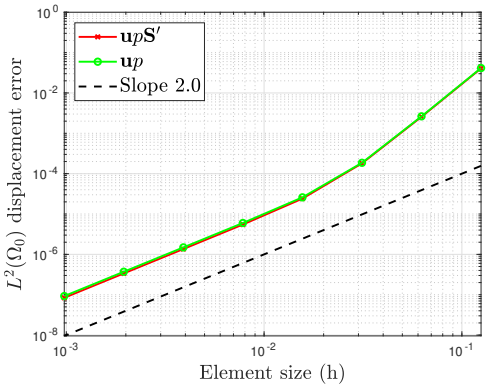

(A) Displacement error upon mesh refinement

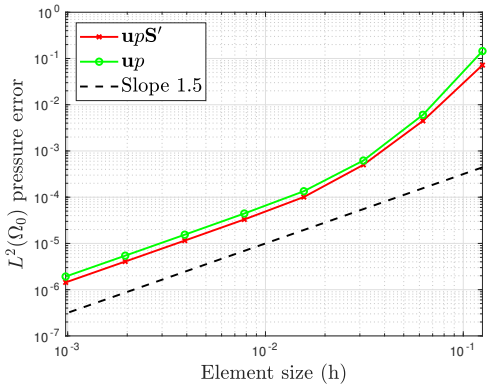

(B) Pressure error upon mesh refinement

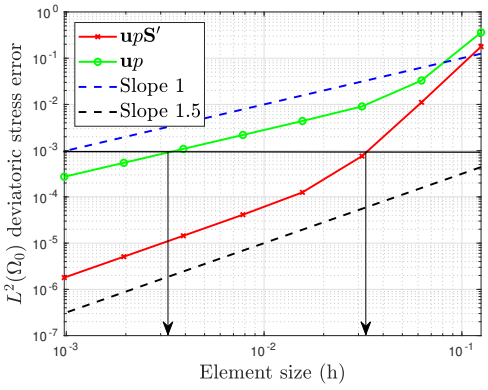

(C) Deviatoric stress error upon mesh refinement

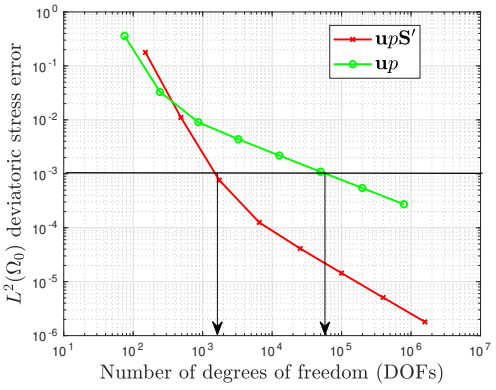

(D) Deviatoric stress error upon number of degrees of freedom

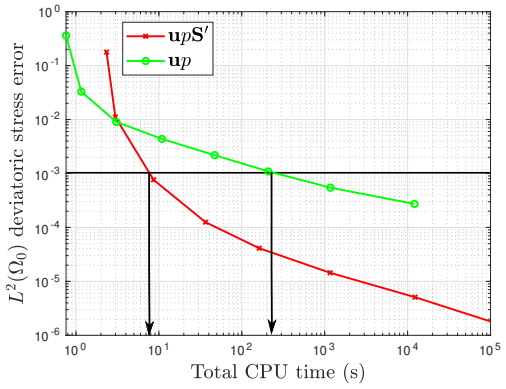

(E) Deviatoric stress error upon CPU time

FIGURE 2. Manufactured convergence test. Comparison of convergence between the $\mathbf{u}p\mathbf{S}'$ formulation and the $\mathbf{u}p$ formulation

Mesh	Number of elements
1	$6 \times 6 \times 36 \times 6$
2	$8 \times 8 \times 48 \times 6$
3	$12 \times 12 \times 72 \times 6$

TABLE 1. Bending Beam. Different mesh and number of elements.

More interesting results are obtained when comparing these convergence rates with respect to the ones obtained with the mixed $\mathbf{u}p$ formulation. Figs 2a-2b show the displacement and pressure convergence rates upon mesh refinement, respectively. Both fields are considered as primary unknowns of both formulations and therefore a similar accuracy for a given mesh size can be expected. Fig. 2c displays the deviatoric PK2 stress convergence rates upon mesh refinement for both formulations. As expected, higher accuracy is achieved for a given mesh size for the mixed $\mathbf{u}p\mathbf{S}'$ formulation. To achieve the same accuracy, e.g. 0.1% of global error, the $\mathbf{u}p$ formulation requires a mesh size, h, almost 10 times finer ($h \approx 0.003$) than the $\mathbf{u}p\mathbf{S}'$ formulation ($h \approx 0.03$) as it can be seen in Fig. 2c.

Furthermore, to obtain a fairer comparison, the same study is conducted in terms of the number of degrees of freedom (DOFs) in Fig. 2d. To get an error lower than 0.1%, the $\mathbf{u}p$ formulation requires $6 \cdot 10^4$ DOFs approximately, while the $\mathbf{u}p\mathbf{S}'$ formulation needs less than $2 \cdot 10^3$ DOFs (25 times lesser than the $\mathbf{u}p$ formulation). Results clearly show that both the $\mathbf{u}p\mathbf{S}'$ and the $\mathbf{u}p$ formulations deal appropriately with the incompressibility constraint but the three-field formulation exhibits a higher accuracy in the stress field, even for very coarse meshes.

For the sake of exhaustiveness, Fig. 2e depicts the total CPU time needed by each FE technology to achieve a given global deviatoric stress accuracy. In particular, to reduce the simulation error below 0.1%, the $\mathbf{u}p\mathbf{S}'$ formulation is more or less 10 times faster compared to the $\mathbf{u}p$ one.

Remark 4.1. *Note that the* $\mathbf{u}p$ *formulation computes the stresses (locally) at the numerical integration points, while the* $\mathbf{u}p\mathbf{S}'$ *formulation adopts a continuous stress field. To compare stress accuracy, a local smoothing technique has been applied to the original discontinuous stress fields of the mixed two-field formulation. So, Figs. 2c-2d-2e present the continuous values obtained after the smoothing operation.*

4.2. **Bending beam.** As a second test in finite strain elasticity, we consider a three dimensional beam of square section clamped on its bottom face very similar to the one presented in [25, 35]. The initial geometry is a thick column of dimensions $1 \times 1 \times 6$ m as shown in Fig. 3a. We consider stress free conditions in all boundaries except the clamped one in which zero displacement is imposed. An initial linear in space velocity field $\mathbf{v}^0(X, Y, Z) = \left(\frac{5}{3}Z, 0, 0\right)^T$ m/s is imposed so as to start the column oscillations in time, leading to a large oscillatory bending deformation.

A Mooney-Rivlin material with initial density $\rho_0 = 1.1 \times 10^3$ kg/m^3 and material parameters $\alpha_1 = 2.69$ MPa and $\alpha_2 = 0.142$ MPa is considered. In order to avoid unphysical modes appearing from the time integration scheme, we have selected the mildly-dissipative BDF2 time integrator with time step $\delta t = 0.01$ s.

The main goal of this example is to show that our stabilized mixed formulation works properly in bending dominated scenarios and in 3D cases. For this reason, we have selected 3 different structured linear tetrahedral meshes (as the one shown in Fig. 3b), specified in Table 1.

Let us start showing some interesting properties about the three-field mixed $\mathbf{u}p\mathbf{S}'$ formulation presented here with respect to the classical displacement-based formulation [36]

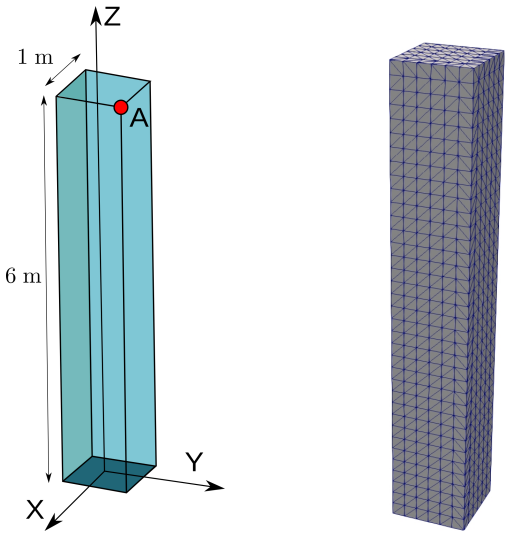

(A) Geometry (B) Mesh

FIGURE 3. Bending Beam. Geometry (3a) and tetrahedral structured mesh (3b).

(from now on named as **u** formulation). To do so, let us consider the bending beam problem for several compressible regimes. We consider 3 differents scenarios: $\nu = 0.2$, which reproduces a compressible material, $\nu = 0.49$, which mimics a nearly incompressible material and finally, we take $\nu = 0.5$ to reach the incompressible limit. All these cases are performed with Mesh 2. Fig. 4a displays the evolution in time up to $T = 3$ for the first component of the displacement field at point A. As expected, in the compressible regime ($\nu = 0.2$), both formulations exhibit very similar results. More interesting conclusions can be drawn when moving to the nearly incompressible regime ($\nu = 0.49$). In such case, the displacement-based formulation presents volumetric locking, which tends to show smaller displacements than the expected ones. On the contrary, the $\mathbf{u}p\mathbf{S}'$ formulation is able to obtain proper solutions without presenting these instabilities. Furthermore, in the incompressible limit ($\nu = 0.5$), the $\mathbf{u}p\mathbf{S}'$ formulation gives us precise solutions whereas the **u** formulation fails over the running stage. To end up this study, Figs. 4b-4c-4d show the pressure field and some components of the deviatoric PK2 stress tensor run with the $\mathbf{u}p\mathbf{S}'$ formulation. As it can be clearly seen, well-defined solutions are obtained regardless the incompressibility of the material and no oscillations can be appreciated even for this coarse mesh.

From now on, let us consider a fully incompressible material with $\nu = 0.5$. Fig. 5 presents the evolution of point A along time up to $T = 3$ s for both $\mathbf{u}p$ and $\mathbf{u}p\mathbf{S}'$ formulations. Figs. 5a-5b show the $L^2(\Omega_0)$ norm for the displacement field and the pressure field, respectively. As previously commented, both unknowns are considered as main variables of the problem. Very similar results can be observed for the displacement field when comparing both formulations for a fixed mesh. Despite the fact that the pressure field is a master field for both formulations, it turns out that more accurate results are obtained for the $\mathbf{u}p\mathbf{S}'$ formulation for a fixed mesh due to the capability of the method to capture stress concentrations better than the $\mathbf{u}p$ formulation. It is interesting to remark, that the observed behavior seems to be more dissipative in the three-field formulation. This indicates that including the deviatoric PK2 stress tensor as unknown of the problem in the $\mathbf{u}p\mathbf{S}'$ formulation both enhances the accuracy of the solution and its energy dissipation rate. On the contrary the $\mathbf{u}p$ formulation shows a less optimal dissipative behavior for the same mesh. Furthermore, Fig. 5c presents the evolution for the $L^2(\Omega_0)$ norm for

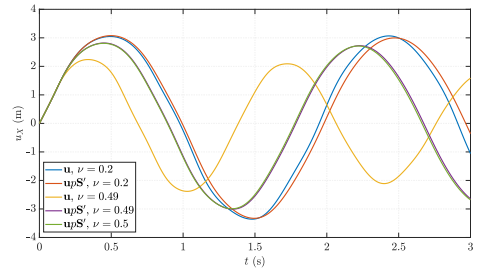

(A) X-Displacement component (m)

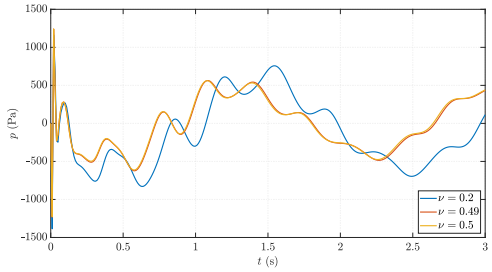

(B) Pressure (Pa)

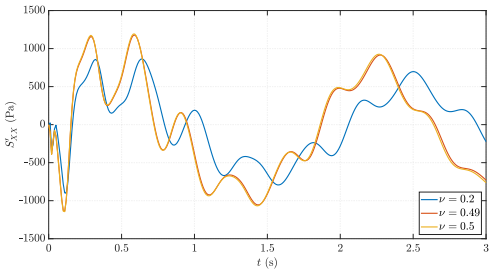

(C) XX-Deviatoric PK2 stress component (Pa)

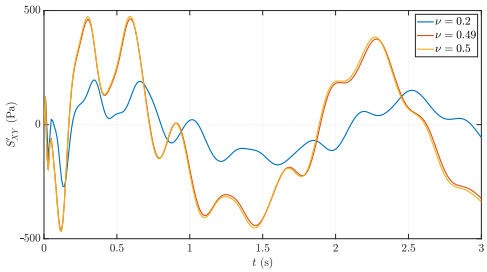

(D) XY-Deviatoric PK2 stress component (Pa)

FIGURE 4. Bending beam. Comparison between $\mathbf{u}$ and $\mathbf{up}\mathbf{S}'$ formulations while increasing the incompressibility of the material at point A.

the deviatoric PK2 stress field. As expected, for a fixed mesh, more accurate results are obtained when introducing the deviatoric PK2 stresses $\mathbf{S}'$ as an extra unknown of the problem in the three-field formulation.

For the sake of thoroughness, we show in Figs. 6-7 the deformed beam at $t = 2.25$ s and at $t = 3$ s, respectively run with Mesh 1. First of all, we can observe that very similar deformations and pressure fields are appreciated for both formulations. Finally, regarding the deviatoric PK2 stress tensor, one can see the gain of accuracy in this field for the $\mathbf{up}\mathbf{S}'$ formulation by including this field as primary unknown of the problem instead of computing it from the displacement derivatives.

4.3. **Twisting column.** As a final example, we present the twisting column test. This test is widely used to assess the robustness of any formulation in extreme nonlinear deformations [25, 26, 35, 49, 50]. The initial geometry of the column is the same as the one shown in Fig. 3a. We consider stress free conditions and zero displacement initial conditions are applied on the corresponding boundaries. In order to make the column twist, we apply an initial sinusoidal velocity field:

$$\mathbf{v}^0\left(X,Y,Z\right) = \omega\, \sin\left(\frac{\pi Z}{12}\right)\left(Y,-X,0\right)^T \quad \text{m/s} \tag{66}$$

where $\omega = 100$ rad/s. The material is considered to be Neo-Hookean with initial density $\rho_0 = 1.1 \times 10^3$ kg/m^3, shear modulus $\mu = 5.7 \times 10^6$ Pa and Poisson ratio $\nu = 0.5$, to model a fully incompressible material. To define the deviatoric part of the material, we consider a Simo-Taylor law. Several levels of refinement have been considered to perform the computations. To construct the meshes, we select structured hexahedral elements. So we consider 3 different meshes. Mesh 1, with $6 \times 6 \times 36$ trilinear FEs, Mesh 2 with $16 \times 16 \times 96$ FEs and we end up with Mesh 3 with $32 \times 32 \times 192$ FEs. We select a time step $\delta t = 0.002$ s.

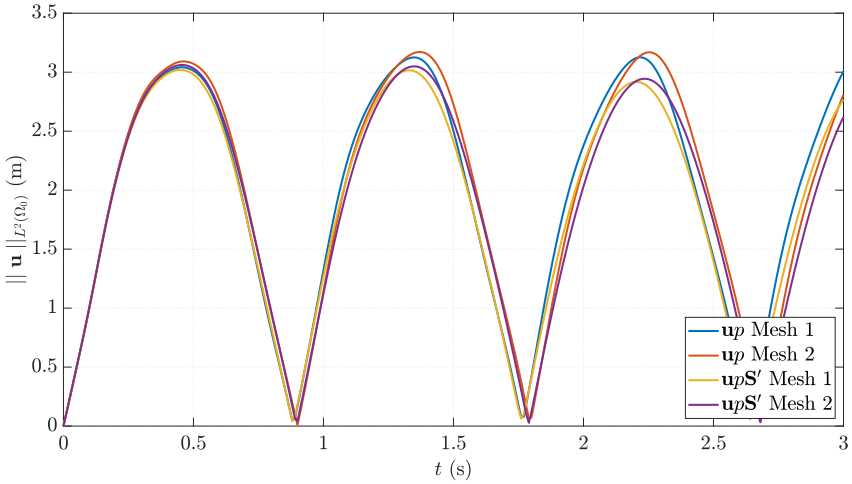

(A) $L^2(\Omega_0)$ norm displacement (m)

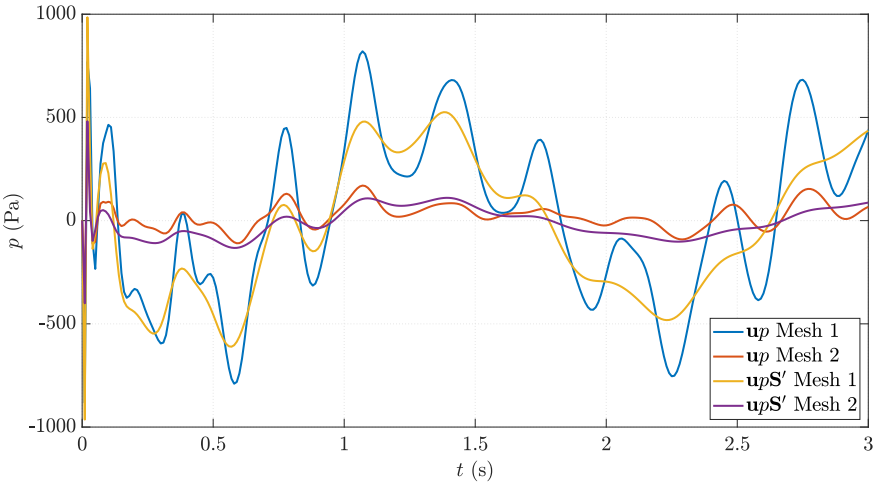

(B) Pressure (Pa)

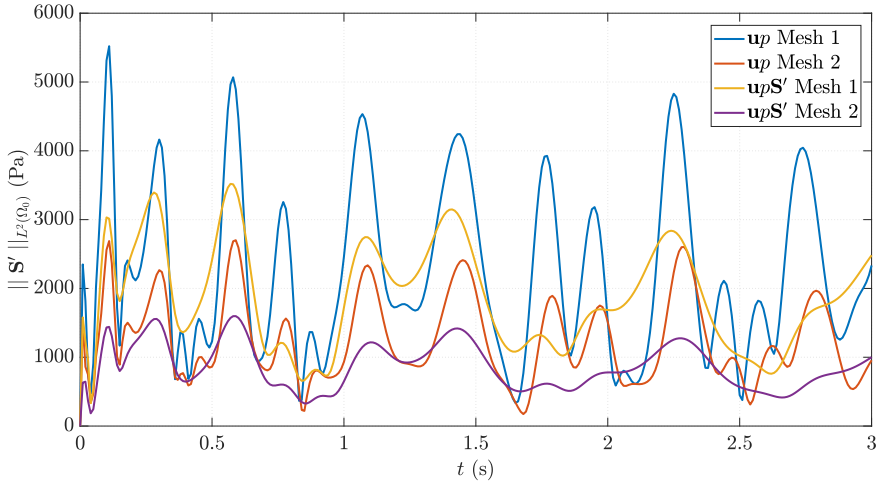

(C) $L^2(\Omega_0)$ norm deviatoric PK2 stress (Pa)

FIGURE 5. Bending beam. Evolution of point A along time for both $\mathbf{u}p$ and $\mathbf{u}p\mathbf{S}'$ formulations.

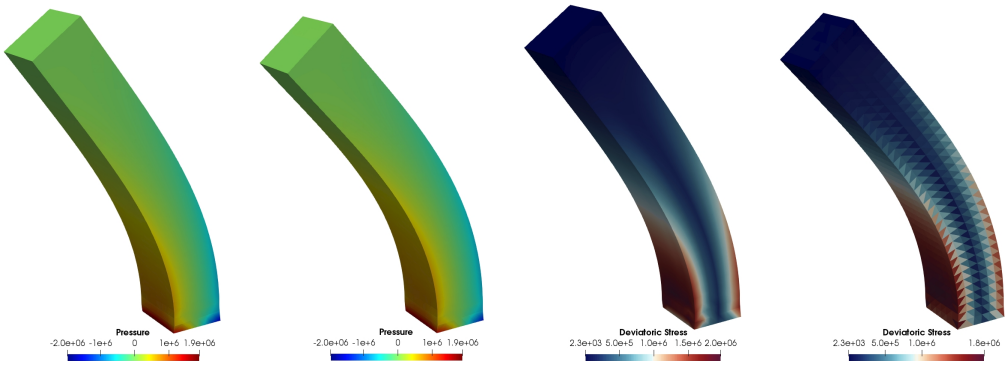

(A) $\mathbf{u}p\mathbf{S}'$ (B) $\mathbf{u}p$ (C) $\mathbf{u}p\mathbf{S}'$ (D) $\mathbf{u}p$

FIGURE 6. Bending beam. Comparison between $\mathbf{u}p\mathbf{S}'$ and $\mathbf{u}p$ at $t = 2.25$ s. Pressure field (Pa) and $L^2(\Omega_0)$ norm of the deviatoric PK2 stress (Pa)

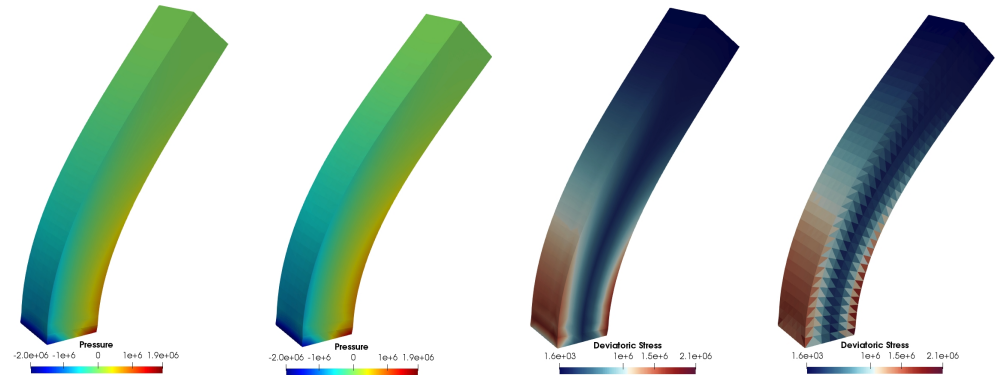

(A) $\mathbf{u}p\mathbf{S}'$ (B) $\mathbf{u}p$ (C) $\mathbf{u}p\mathbf{S}'$ (D) $\mathbf{u}p$

FIGURE 7. Bending beam. Comparison between $\mathbf{u}p\mathbf{S}'$ and $\mathbf{u}p$ at $t = 3$ s. Pressure field (Pa) and $L^2(\Omega_0)$ norm of the deviatoric PK2 stress (Pa)

First of all, let us perform some analysis for the different time integration schemes presented in Section 2. We run the same problem with different schemes and Mesh 2 and the main results can be seen in Fig. 8. On the one hand, left figures display the main unknowns up to $T = 0.5$ s. As it can be seen, both BDF schemes are capable of reproducing the whole event. However, BDF1 is only first-order accurate in time and it is highly dissipative, excessively mitigating physical oscillations. With regards to the BDF2 scheme, it is able to dissipate the nonphysical modes, which helps preventing high frequency oscillations while keeping the second-order accuracy of the method. On the other hand, right figures illustrate the evolution obtained with a Newmark scheme for $\beta = \frac{1}{4}$ and $\gamma = \frac{1}{2}$, which results in a second-order scheme in time. This method does not introduce any numerical dissipation, and therefore, it does not eliminate high frequency nonphysical oscillations.

Next, let us fix BDF2 as time integration scheme and perform some comparisons between the $\mathbf{u}p$ and the $\mathbf{u}p\mathbf{S}'$ formulations. Fig. 9 shows the evolution of point A up to $T = 0.5$ s. In Fig. 9a we can observe a comparison for the displacement field. As expected, both formulations show very similar results, which become closer upon mesh refinement. Moving to the pressure field in Fig. 9b, one can see that for a fixed mesh, similar evolutions are obtained but the $\mathbf{u}p\mathbf{S}'$ formulation gives more accurate results taking into account the evolution when refining the mesh. More interesting remarks can be made for the deviatoric

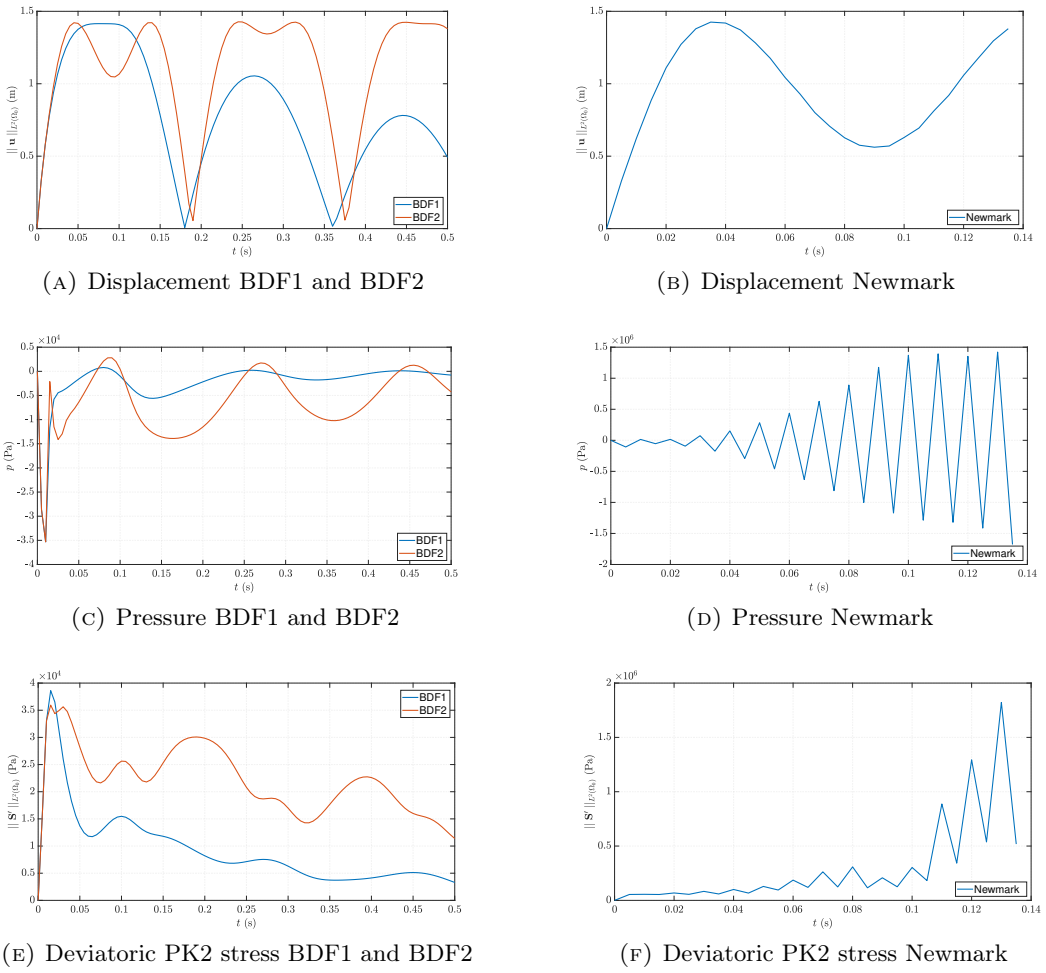

(A) Displacement BDF1 and BDF2

(B) Displacement Newmark

(C) Pressure BDF1 and BDF2

(D) Pressure Newmark

(E) Deviatoric PK2 stress BDF1 and BDF2

(F) Deviatoric PK2 stress Newmark

FIGURE 8. Twisting column. Time integrators comparison.

PK2 stress tensor in Fig 9c. As it can be clearly appreciated, for a fixed mesh the three-field formulation attains more accurate results than the two-field version of the problem. In fact, we can observe that we need always an extra level of refinement for the $\mathbf{u}p$ formulation to be able to achieve the same accuracy as the one given by the $\mathbf{u}p\mathbf{S}'$ formulation.

To complete this example, Figs. 10-11 display the evolution of the deformation for the twisting column at different stages of the problem with Mesh 2. As it can be observed, the problem is well-captured, and no numerical oscillations can be seen neither for the pressure field nor for the deviatoric PK2 stress tensor. Let us remark, once more, the capability of the formulation to capture stress concentrations, in this case, placed at the clamped face of the twisting column.

5. CONCLUSIONS

In this paper we have described a new stabilized FE method for stress accurate analysis in solid dynamics when considering nearly and fully incompressible materials. The point of departure is the splitting of the Cauchy stress tensor into deviatoric and spherical components, which then translates into a splitting of the second Piola–Kirchhoff stress tensor.

The momentum equation is complemented with a constitutive law for the pressure which emerges from the deviatoric/volumetric decomposition of the strain energy function for

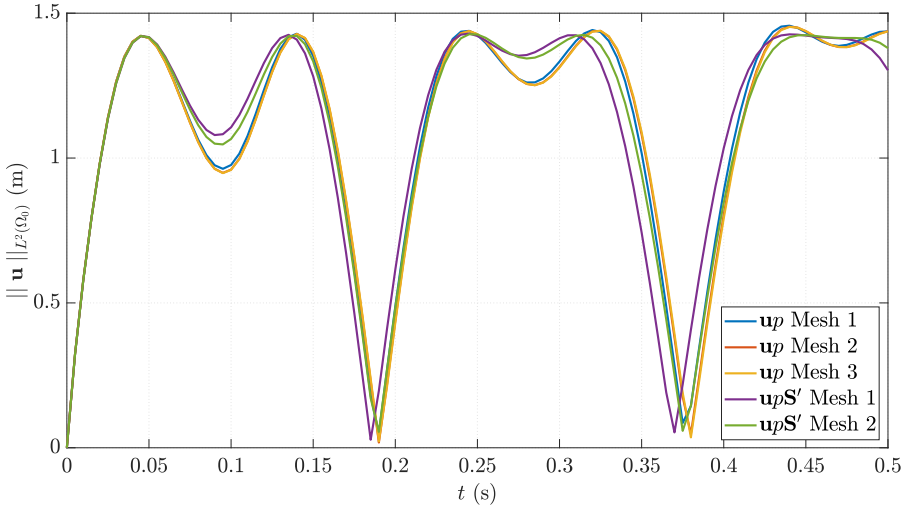

(A) $L^2(\Omega_0)$ norm displacement (m)

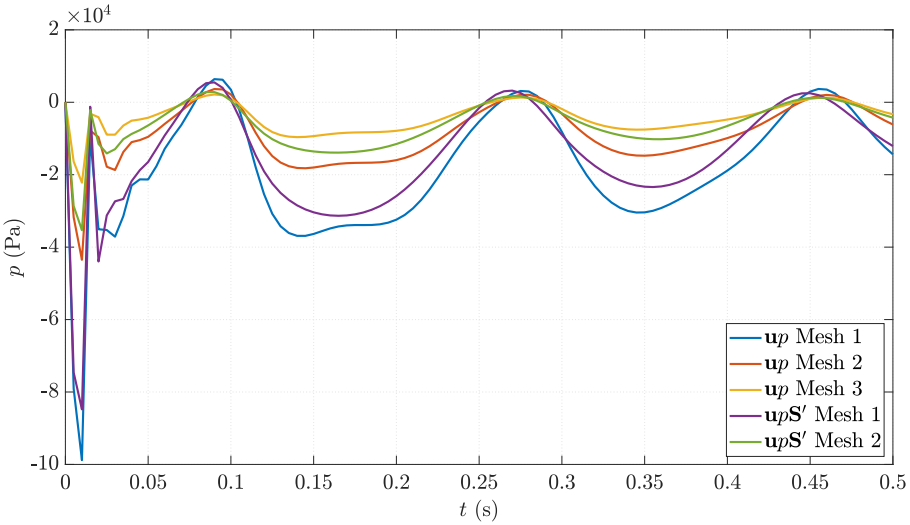

(B) Pressure

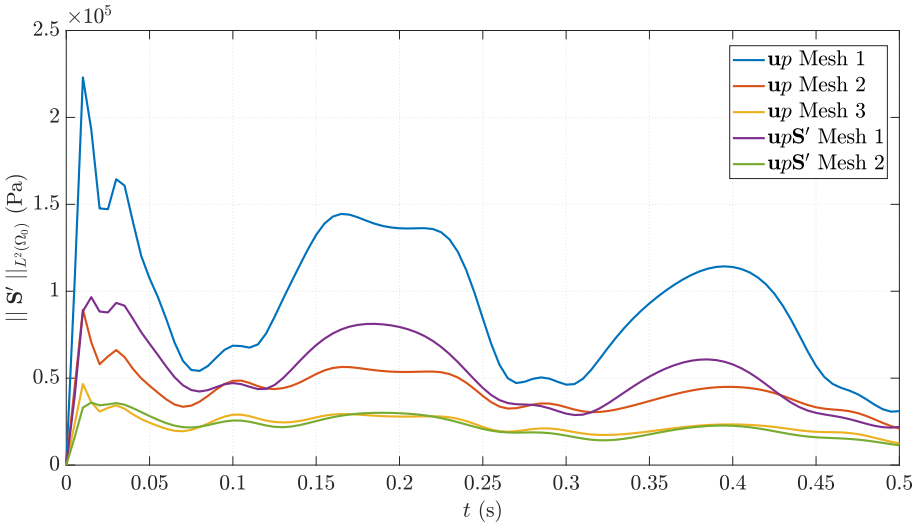

(C) $L^2(\Omega_0)$ norm deviatoric PK2 stress (Pa)

FIGURE 9. Twisting column. Evolution at point A.

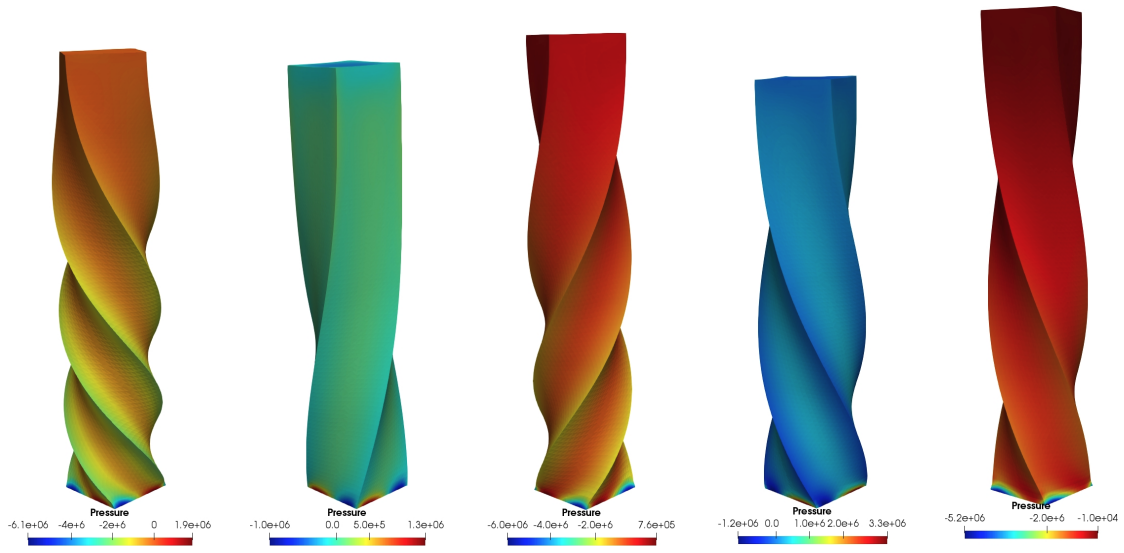

(A) 0.1 s (B) 0.2 s (C) 0.3 s (D) 0.4 s (E) 0.5 s

FIGURE 10. Twisting column. Deformation and Pressure field (Pa) along time.

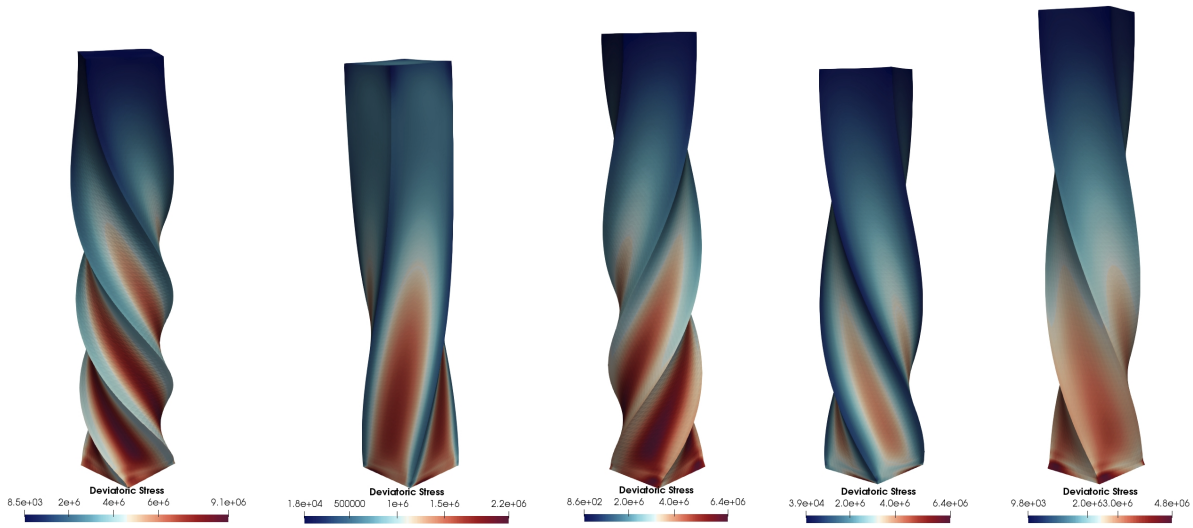

(A) 0.1 s (B) 0.2 s (C) 0.3 s (D) 0.4 s (E) 0.5 s

FIGURE 11. Twisting column. Deformation and $L^2(\Omega_0)$ norm deviatoric PK2 stress (Pa) along time.

any hyperelastic material model. This law is formulated properly to obtain a simple way to impose the incompressibility of the material automatically. Furthermore, to design a FE technology with a high degree of accuracy of the stress field, the constitutive law for deviatoric stresses is added to the system to obtain a monolithic system of equations for the displacement/pressure/deviatoric stress formulation. The presented three-field approach is able to deal with any hyperelastic material, including fully incompressible cases.

We have proposed two residual-based (ASGS and OSGS) and a term-by-term (S-OSGS) type stabilization techniques based on the decomposition of the unknowns into FE scales and SGSs. All stabilization techniques are able to circumvent the compatibility restrictions on the interpolation functions among the primary unknowns of the problem. Furthermore,

the proposed scheme shows the desired rate of convergence upon mesh refinement regardless the stabilization technique. It is interesting to remark that the S-OSGS stabilization technique allows us to obtain well-defined solutions and to neglect terms that do not contribute to stability. This methods turns out to be more robust for solving problems when large stress gradients are present. Likewise, for the examples we have considered, we have been able to assume quasi-static SGSs, although dynamic SGSs might need to be considered if very small time step sizes are required.

Concerning the computational cost of the method, we have observed that the proposed methods display quadratic non-linear convergence regardless the stabilization technique, as it is expected from the implementation of a Newton–Raphson iterative procedure. The proposed three-field formulation is convergent upon mesh refinement, virtually free of any volumetric or shear locking. The technology is suitable for engineering applications in which a higher accuracy of stresses is needed. A comparison with the two-field formulation (displacement/pressure) is also carried out. Results clearly show that both the $\mathbf{u}p\mathbf{S}'$ and the $\mathbf{u}p$ formulations deal appropriately with the incompressibility constraint but the three-field formulation exhibits a higher accuracy in the stress field, even for very coarse meshes.

Acknowledgements

Inocencio Castañar gratefully acknowledges the support received from the Agència de Gestió d'Ajut i de Recerca through the predoctoral FI grant 2019-FI-B-00649. R. Codina gratefully acknowledges the support received through the ICREA Acadèmia Research Program of the Catalan Government. This work was partially funded through the TOP-FSI: RTI2018-098276-B-I00 project of the Spanish Government.

References

[1] C.A. Moreira, G.B. Barbat, M. Cervera, and M. Chiumenti. Accurate thermal-induced structural failure analysis under incompressible conditions. *Engineering Structures*, 261:114213, 2022.

[2] N. Dialami, M. Chiumenti, and M. Cervera. Defect formation and material flow in friction stir welding. *European Journal of Mechanics A / Solids*, 80:103912, 2020.

[3] M. Cervera, M. Chiumenti, and R. Codina. Mixed stabilized finite element methods in nonlinear solid mechanics. Part II: Strain localization. *Computer Methods in Applied Mechanics and Engineering*, 199(37–40):2571–2589, 2010.

[4] M. Cervera, G.B. Barbat, M. Chiumenti, and J.Y. Wu. A comparative review of xfem, mixed fem and phase-field models for quasi-brittle cracking. *Archives of Computational Methods in Engineering*, 29:1009–1083, 2022.

[5] M. Chiumenti, M. Cervera, C.A. Moreira, and G.B. Barbat. Stress, strain and dissipation accurate 3-field formulation for inelastic isochoric deformation. *Finite Elements in Analysis and Design*, 192:103534, 2021.

[6] G. A. Holzapfel. *Nonlinear solid mechanics. A continuum approach for engineering*. Wiley, 2000.

[7] G. A. Holzapfel. Biomechanics of soft tissue. *The Handbook of Materials Behavior*, 3:1049–1063, 2001.

[8] P. E. Farrell, L.F. Gatica, B. P. Lamichhane, R. Oyarzúa, and R. Ruiz-Baier. Mixed kirchhoff stress-displacement-pressure formulations for incompressible hyperelasticity. *Computer Methods in Applied Mechanics and Engineering*, 374:113562, 2021.

[9] R. Ruiz-Baier, A. Gizzi, A. Loppini, C. Cherubini, and S. Filippi. Thermo-electric effects in an anisotropic active-strain electromechanical model. *Communications in Computational Physics*, 27(1):87–115, 2020.

[10] A. Propp, A. Gizzi, F. Levrero-Florencio, and R. Ruiz-Baier. An orthotropic electro-viscoelastic model for the heart with stress-assisted diffusion. *Biomechanics and Modeling in Mechanobiology*, 19(2):633–659, 2020.

[11] T. Belytschko, W. K. Liu, and B. Moran. *Nonlinear Finite Elements for Continua and Structures*. Wiley, 2001.

[12] T. J. R. Hughes. *The Finite Element Method: Linear Static and Dynamic Finite Element Analysis*. Prentice-Hall,Englewood Cliffs, New Jersey, 1987.

[13] D. S. Malkus and T. J. R. Hughes. Mixed finite element methods - Reduced and selective integration techniques: A unification of concepts. *Computer Methods in Applied Mechanics and Engineering*, 15:63–81, 1978.

[14] T. Elguedj, Y. Bazilevs, V. M. Calo, and T. J. R. Hughes. $\bar{B}$ and $\bar{F}$ projection methods for nearly incompressible linear and nonlinear elasticity and plasticity using higher-order NURBS elements. *Computer Methods in Applied Mechanics and Engineering*, 197:2732–2762, 2008.

[15] T. J. R. Hughes, G. R. Feijóo, L. Mazzei, and J. Quincy. The variational multiscale method - A paradigm for computational mechanics. *Computer Methods in Applied Mechanics and Engineering*, 166:3–24, 1998.

[16] R. Codina. Stabilized finite element approximation of transient incompressible flows using orthogonal subscales. *Computer Methods in Applied Mechanics and Engineering*, 191:4295–4321, 2002.

[17] R. Codina. Finite element approximation of the three field formulation of the Stokes problem using arbitrary interpolations. *SIAM Journal on Numerical Analysis*, 47:699–718, 2009.

[18] S. Badia and R. Codina. Unified stabilized finite element formulations for the Stokes and the Darcy problems. *SIAM Journal on Numerical Analysis*, 47(3):1971–2000, 2009.

[19] M. Cervera, M. Chiumenti, and R. Codina. Mixed stabilized finite element methods in nonlinear solid mechanics. Part I: Formulation. *Computer Methods in Applied Mechanics and Engineering*, 199(37–40):2559–2570, 2010.

[20] J. Baiges and R. Codina. Variational multiscale error estimators for solid mechanics adaptive simulations: an orthogonal subgrid scale approach. *Computer Methods in Applied Mechanics and Engineering*, 325:37–55, 2017.

[21] M. Chiumenti, Q. Valverde, C.A. de Saracibar, and M. Cervera. A stabilized formulation for incompressible elasticity using linear displacement and pressure interpolations. *Computer Methods in Applied Mechanics and Engineering*, 191:1095–1116, 2002.

[22] R. Codina and O. Turk. Modal analysis of elastic vibrations of incompressible materials using a pressure-stabilized finite element method. *Finite Elements in Analysis and Design*, 206:103760, 2022.

[23] R. Rossi, R. Zorrilla, and R. Codina. A stabilized displacement-volumetric strain formulation for nearly incompressible and anisotropic materials. *Computer Methods in Applied Mechanics and Engineering*, 377:113701, 2021.

[24] M. Chiumenti, M. Cervera, and R. Codina. A mixed three-field FE formulation for stress accurate analysis including the incompressible limit. *Computer Methods in Applied Mechanics and Engineering*, 283:1095–1116, 2015.

[25] G. Scovazzi, B. Carnes, X. Zeng, and S. Rossi. A simple, stable, and accurate linear tetrahedral finite element for transient, nearly, and fully incompressible solid dynamics: a dynamic variational multiscale approach. *International Journal For Numerical Methods in Engineering*, 106:799–839, 2016.

[26] S. Rossi, N. Abboud, and G. Scovazzi. Implicit finite incompressible elastodynamics with linear finite elements: A stabilized method in rate form. *Computer Methods in Applied Mechanics and Engineering*, 311:208–249, 2016.

[27] C. H. Lee, A. J. Gil, and J. Bonet. Development of a cell centred upwind finite volume algorithm for a new conservation law formulation in structural dynamics. *Computers and Structures*, 118:13–38, 2013.

[28] C.H. Lee, A. J. Gil, and J. Bonet. Development of a stabilised Petrov-Galerkin formulation for linear tetrahedral elements in compressible, nearly incompressible and truly incompressible fast dynamics. *Computer Methods in Applied Mechanics and Engineering*, 268:40–64, 2014.

[29] C.H. Lee, A. J. Gil, J. Bonet, and M. Aguirre. A stabilised Petrov-Galerkin formulation for linear tetrahedral elements in compressible, nearly incompressible and truly incompressiblefast dynamics. *Computer Methods in Applied Mechanics and Engineering*, 276:659–690, 2014.

[30] M. Aguirre, A. J. Gil, J. Bonet, and A. Arranz-Carreño. A vertex centred finite volume Jameson-Schmidt-Turkel (JST) algorithm for a mixed conservation formulation in solid dynamics. *Journal of Computational Physics*, 259:672–699, 2014.

[31] M. Aguirre, A. J. Gil, J. Bonet, and C. H. Lee. An upwind vertex centred finite volume solver for Lagrangian solid dynamics. *Journal of Computational Physics*, 300:387–422, 2015.

[32] C. H. Lee J. Haider, A. J. Gil, and J. Bonet. A first-order hyperbolic framework for large strain computational solid dynamics. An upwind cell centred Total Lagrangian scheme. *International Journal for Numerical Methods in Engineering*, 109:407–456, 2017.

[33] R. Nemer, A. Larcher, T. Coupez, and E. Hachem. Stabilized finite element method for incompressible solid dynamics using an updated Lagrangian formulation. *Computer Methods in Applied Mechanics and Engineering*, 384:113923, 2021.

[34] W. Boscheri, R. Loubère, and P. Maire. A 3d cell-centered ADER MOOD finite volume method for solving updated Lagrangian hyperelasticity on unstructured grids. *Journal of Computational Physics*, 449:110779, 2022.

[35] I. Castañar, J. Baiges, and R. Codina. A stabilized mixed finite element approximation for incompressible finite strain solid dynamics using a total Lagrangian formulation. *Computer Methods in Applied Mechanics and Engineering*, 368:113164, 2020.

[36] J. Bonet and R.D. Wood. *Nonlinear Continuum mechanics for finite element analysis*. Cambridge University Press, 1997.

[37] C. O. Horgan and J. G. Murphy. On the volumetric part of strain-energy functions used in the constitutive modeling of slightly compressible solid rubbers. *International Journal of Solids and Structures*, 46:3028–3085, 2009.

[38] J.C. Simo, R.L. Taylor, and K.S. Pister. Variational and projection methods for the volume constraint in finite deformation elasto-plasticity. *Computer Methods in Applied Mechanics and Engineering*, 51(1–3):177–208, 1985.

[39] T. Belytschko and D. F. Schoeberle. On the unconditional stability of an implicit algorithm for nonlinear structural dynamics. *Journal of Applied Mechanics*, 42(4):865–869, 1975.

[40] J. C. Simo, N. Tarnow, and K. K. Wong. Exact energy-momentum conserving algorithms and symplectic schemes for nonlinear dynamics. *Computer Methods in Applied Mechanics and Engineering*, 100(1):63–116, 1992.

[41] O. Gonzalez. Exact energy and momentum conserving algorithms for general models in nonlinear elasticity. *Computer Methods in Applied Mechanics and Engineering*, 190:1763–1783, 2000.

[42] P. Betsch and A. Janz. An energy–momentum consistent method for transient simulations with mixed finite elements developed in the framework of geometrically exact shells. *International Journal of Numerical Methods in Engineering*, 108(5):423–455, 2016.

[43] D. Magisano, L. Leonetti, and G. Garcea. Unconditional stability in large deformation dynamic analysis of elastic structures with arbitrary nonlinear strain measure and multi-body coupling. *Computer Methods in Applied Mechanics and Engineering*, 393:114776, 2022.

[44] I. Babuška. Error-bounds for finite element method. *Numerische Mathematik*, 16(4):322–333, 1971.

[45] R. Codina, S. Badia, J. Baiges, and J. Principe. *Variational Multiscale Methods in Computational Fluid Dynamics,* in Encyclopedia of Computational Mechanics, pages 1–28. John Wiley & Sons Ltd., 2017.

[46] R. Codina, J. M. González-Ondina, G. Díaz-Hernández, and J. Príncipe. Finite element approximation of the modified Boussinesq equations using a stabilized formulation. *International Journal For Numerical Methods in Engineering*, 57:1249–1268, 2008.

[47] R. Codina. Stabilization of incompressibility and convection through orthogonal sub-scales in finite element methods. *Computer Methods in Applied Mechanics and Engineering*, 190:1579–1599, 2000.

[48] L. Moreno, R. Codina, J. Baiges, and E. Castillo. Logarithmic conformation reformulation in viscoelastic flow problems approximated by a vms-type stabilized finite element formulation. *Computer Methods in Applied Mechanics and Engineering*, 354:706–731, 2019.

[49] J. Bonet, A. J. Gil, C. H. Lee, M. Aguirre, and R. Ortigosa. A first order hyperbolic framework for large strain computational solid dynamics. Part I : Total Lagrangian isothermal elasticity. *Computer Methods in Applied Mechanics and Engineering*, 283:689–732, 2015.

[50] A. J. Gil, C. H. Lee, J. Bonet, and R. Ortigosa. A first order hyperbolic framework for large strain computational solid dynamics. Part II : Total Lagrangian compressible, nearly incompressible and truly incompressible elasticity. *Computer Methods in Applied Mechanics and Engineering*, 300:146–181, 2016.

[51] H. A. Van der Vorst. Bi-CGSTAB: A fast and smoothly converging variant of Bi-CG for the solution of nonsymmetric linear systems. *SIAM, Journal of Scientific and Statistical Computing*, 13(2):631 – 644, 1992.

[52] S.Balay, S. Abhyankar, M. F. Adams, J. Brown, P. Brune, K. Buschelman, L. Dalcin, V. Eijkhout, W. D. Gropp, D. Kaushik, M. G. Knepley, D. A. May, L. Curfman McInnes, R. T. Mills, T. Munson, K. Rupp, P. Sanan, B. F. Smith, S. Zampini, H. Zhang, and H. Zhang. PETSc Web page, http://www.mcs.anl.gov/petsc, 2015.

[53] C. Miehe. Aspects of the formulation and finite element implementation of large strain isotropic elasticity. *International Journal for Numerical Methods in Engineering*, 12:1981–2004, 1994.

[54] C. H. Liu, G. Hofstetter, and H. A. Mang. 3D finite element analysis of rubber-like materials at finite strains. *Engineering Computations*, 11(2):111–128, 1994.

[55] L. P. Franca, T. J. R. Hughes, A. F. D. Loula, and I. Miranda. A new family of stable elements for nearly incompressible elasticity based on a mixed Petrov-Galerkin finite element formulation. *Numerische Mathematik*, 53(1–2):123–141, 1988.

[56] J. Bonet and A. J. Burton. A simple average nodal pressure tetrahedral element for incompressible and nearly incompressible dynamic explicit applications. *Computer Methods in Applied Mechanics and Engineering*, 1(4):437–449, 1998.

[57] O. I. Hassan, A. Ghavamian, C. H. Lee, A. J. Gil, J. Bonet, and F. Auricchio. An upwind vertex centred finite volume algorithm for nearly and truly incompressible explicit fast solid dynamic applications: Total and Updated Lagrangian formulations. *Journal of Computational Physics : X*, 3:100025, 2019.

[58] B. Müller, G. Starke, A. Schwarz, and J. Schröder. A first-order system least squares method for hyperelasticity. *Society for Industrial and Applied Mathematics*, 36(5):B795–B816, 2014.

[59] F. Auricchio, L. B. da Veiga, C. Lovadina, A. Reali, R. L. Taylor, and P. Wriggers. Approximation of incompressible large deformation elastic problems: some unresolved issues. *Computational Mechanics*, 52(5):1153–1167, 2013.

[60] J. Schröder, N. Viebahn, P. Wriggers, F. Auricchio, and K. Steeger. On the stability analysis of hyperelastic boundary value problems using three- and two-field mixed finite element formulations. *Computational Mechanics*, 60:479–492, 2017.

[61] C. Sansour. On the physical assumptions underlying the volumetric-isochoric split and the case of anisotropy. *European Journal of Mechanics A/Solids*, 27:28–39, 2008.

[62] C. Kadapa and M. Hossain. A linearized consistent mixed displacement-pressure formulation for hyperelasticity. *Mechanics of Advanced Materials and Structures*, 29:267–284, 2022.

[63] R. Codina. A stabilized finite element method for generalized stationary incompressible flows. *Computer Methods in Applied Mechanics and Engineering*, 190:2681–2706, 2001.

[64] T. J. R. Hughes, L. P. Franca, and M. Balestra. A new finite element formulation for computational fluid dynamics: V. Circumventing the babuška-brezzi condition: a stable Petrov-Galerkin formulation of the stokes problem accommodating equal-order interpolations. *Computer Methods in Applied Mechanics and Engineering*, 59:85–99, 1986.

[65] X. Oliver and C. A. de Saracibar. *Continuum Mechanics for Engineers. Theory and Problems, 2nd edition.* Universitat Politècnica de Catalunya, 2017.

[66] E. Boman, K. Devine, L. A. Fisk, R. Heaphy, B. Hendrickson, V. Leung, C. Vaughan, U. Catalyurek, D. Bozdag, and W. Mitchell. Zoltan home page, http://www.cs.sandia.gov/zoltan. *Sandia National Laboratories*, 1999.

[67] W. Schroeder, K. Martin, and B. Lorensen. *The Visualization Toolkit (4th ed.).* Kitware, 2006.

[68] J. Chung and G. M. Hulbert. A Time Integration Algorithm for Structural Dynamics with improved numerical dissipation: The generalized-α method. *Journal of Applied Mechanics*, 60(2):371 – 375, 1993.